STRUCTURAL AND FUNCTIONAL DYNAMICS OF *ESCHERICHIA COLI* RIBONUCLEASE II: INITIAL STUDIES USING A NOVEL FLUORESCENCE BASED SYSTEM

ADAM DAVID SMITH
Bachelor of Science, University of Lethbridge, 2005

A Thesis
Submitted to the School of Graduate Studies
of the University of Lethbridge
in Partial Fulfillment of the
Requirements for the Degree

MASTER OF SCIENCE

Department of Chemistry and Biochemistry
University of Lethbridge
LETHBRIDGE, ALBERTA, CANADA

Abstract

Ribonuclease II (RNase II) is a bacterial enzyme responsible for 90% of the exonucleolytic degradation of mRNA in bacteria, and has bacterial homologues known to be involved in virulence. The goal of this project was to examine the structural dynamics of RNase II using fluorescence. Prior to the beginning of this project, little was known regarding the structural composition of RNase II – required information in the study of structural dynamics. Consequently, the structure of RNase II was studied by constructing a series of deletion mutants in order to map the domains. The publication of an atomic resolution structure of RNase II allowed the project to move directly into the study of RNase II structural dynamics as it degrades mRNA. As a step towards this, RNase II was fluorescently labeled, and preliminary binding studies of DNA – a competitive inhibitor – to RNase II using fluorescence were conducted.

Table of Contents Page

Abbreviations Used

2-AP	2-aminopurine
5-IAF	5-iodoacetamidofluorescein
APS	Ammonium persulfate
BAC	Bacterial artificial chromosome
dA(30)	Polymer of 30 deoxyriboadenylic acid residues
dA(30)-2-AP	dA(30) with 2-AP replacing the 6^{th} adenine from the 3' end
dNTP	Deoxyribonucleoside triphosphate
DMSO	Dimethyl sulfoxide
DNA	Deoxyribonucleic acid
DTT	Dithiothreitol
EDTA	Ethylene diamine tetraacetic acid
EMSA	Electrophoretic mobility gel shift assay
FRET	Fluorescence resonance energy transfer
HPLC	High performance liquid chromatography
IPTG	Isopropyl-D-thiogalatopyranoside
LB	Luria-Bertani broth
LPLC	Low pressure liquid chromatography
NiNTA	Nickel nitrilotriacetic acid
PAG	Polyacrylamide gel
PAGE	Polyacrylamide gel electrophoresis
PCR	Polymerase chain reaction

RNA	Ribonucleic acid
RNBec	*Escherichia coli* Ribonuclease II protein
RNBec_N22	*E. coli* Ribonuclease II protein with an N-terminal 22 residue histidine affinity tag
RNBec_N22_c60	*E. coli* Ribonuclease II protein with an N-terminal 22 residue histidine affinity tag and lacking 60 C-terminal residues
RNBec_N22_c170	*E. coli* Ribonuclease II protein with an N-terminal 22 residue histidine affinity tag and lacking 170 C-terminal residues
RNBec_N22*5IAF	*E. coli* Ribonuclease II protein with an N-terminal histidine affinity tag and a 5-IAF fluorescent label
RNBec_N22_D209N	*E. coli* Ribonuclease II protein with an N-terminal histidine affinity label and an aspartate to asparagine mutation at amino acid 209
RNBst_N22	*Salmonella enterica* serovar Typhimurium LT2 Ribonuclease II protein with an N-terminal 22 residue histidine affinity tag
SDS	Sodium dodecyl sulfate
SDS-PAGE	Sodium dodecyl sulfate polyacrylamide gel electrophoresis
SEC	Size exclusion chromatography
SGSC	Salmonella genetic stock centre
TEMED	Tetramethylethylenediamine

TAE	Tris acetate EDTA
TBE	Tris borate EDTA

Chapter 1: Introduction

1.1 Ribonucleic Acid Hydrolysis

There are two pathways for RNA hydrolysis in *Escherichia coli* (*E.coli*). The first is the processing of precursor RNA. Two examples of this are the endonucleolytic cleavage of the 30S precursor ribosomal RNA (rRNA) transcript by Ribonuclease III (RNase III) to generate mature 16S and 23S rRNA (Dunn and Studier, 1973; Young and Steitz, 1978) and the maturation of the 3' end of 5S and 23S rRNA by exonucleolytic trimming by RNase T (Li and Deutscher, 1995; Li et al., 1999). The second major form of RNA hydrolysis is degradative. The purpose of degradative RNA hydrolysis is to reduce mature RNAs which have served their purpose to their nucleotide components.

1.2 Inactivation of mRNA and the Initiation of mRNA Degradation

Messenger RNA (mRNA) degradation in *E.coli* is initiated by an endonucleolytic cleavage. The identification of the enzyme responsible for this is currently a topic of debate (Kennell, 2002; Kushner, 2002). This can be attributed to the multiple endoribonucleases in *E.coli* which have been proposed to initiate mRNA degradation. It is widely believed that the 5' end dependant endoribonuclease (Bouvet and Belasco, 1992) RNase E is primarily responsible for this initial cut (Apirion, 1978). In his review on bacterial mRNA degradation (2002), David Kennell argues that RNase E is not responsible for the majority of mRNA inactivation, based on the works by Kuwano and Ono (1977; 1979). Kennell goes on to argue in favor of the less specific endoribonuclease RNase M as the protein responsible for the initiation of mRNA degradation. While it is at present not completely understood how mRNA degradation is initiated, it is clear that the first step in the degradation of mRNA in *E.coli* is the

inactivation of the message by an endonucleolytic cleavage. In eukaryotic cells, one of the first steps in message inactivation is the removal of the 5' end cap (Weaver, 2002), an element vital for ribosome binding. In *E.coli* however, the initial inactivation by endonucleolytic cleavage does not prevent ribosomes from binding to the Shine-Dalgarno sequence; however, it does prevent ribosomes from translating the entire message, and in this way the message is functionally inactivated. From this point, the message fragments must be reduced to their individual nucleotide components.

1.3 Exonucleolytic RNA degradation

In contrast to the differences in the initiation of mRNA degradation between eukaryotic and prokaryotic systems, there are some similarities between these systems in the final steps of mRNA degradation. Both eukaryotes and prokaryotes have enzymes that can catalyze multiple turnovers of individual nucleotide removal from an RNA chain without dissociating. The vast majority of these enzymes remove individual nucleotides from the 3' end of RNA. The enzymes that have these properties are termed 3'-5' processive exoribonucleases. A variety of 3'-5' processive exoribonucleases are implicated in the breakdown of mRNAs to ribonucleoside 5' monophosphates in eukaryotic, archaeal and prokaryotic systems (Gupta et al., 1977; Kivity-Vogel and Elson, 1968; Lorentzen and Conti, 2005; Mitchell et al., 1997; Navarro et al., 2008; Spahr and Schlessinger, 1963), often with multiple 3'-5' processive exoribonucleases in the same organism. The specific function of each of these proteins is poorly understood aside from their role in degrading bulk mRNA and protecting against the devastating effect of a total loss of free nucleotides that would occur as a result of the inactivation of all mRNA degradation machinery.

1.3.1 Exonucleolytic RNA Degradation in Eukaryotes and Archaea

In eukaryotic and archaeal organisms, 3'-5' processive exoribonucleolytic degradation is primarily mediated by a multienzyme complex termed the exosome (Evguenieva-Hackenberg et al., 2003; Mitchell et al., 1997). In some cases, the exoribonuclease activity of the exosome originates from its core components, while in others, the exosome is an apoenzyme termed the core exosome, and requires additional proteins in order to form the holoenzyme.

Core exosomes that have been structurally characterized (Liu et al., 2006; Lorentzen and Conti, 2005; Lorentzen et al., 2007; Lorentzen et al., 2005; Navarro et al., 2008; Wang et al., 2007) have a number of features in common. In most organisms the core exosome is composed of a six-member protein ring with three capping proteins. The members of the ring, Rrp41-like and Rrp42-like proteins, are all RNase PH homologues (a phosphorolytic 3'-5' processive exoribonuclease). The three capping proteins are RNA-binding proteins and are located on the RNA entry side of the ring (Figure 1A). The hexameric ring can be more accurately described as a trimer of heterodimers, with each heterodimer composed of one Rrp41-like monomer and one Rrp42-like monomer arranged in an anti-parallel orientation. The dimer interface on the inside of the ring structure creates a positively charged channel to which the RNA strand is proposed to bind (Evguenieva-Hackenberg et al., 2003; Liu et al., 2006). Despite very similar structures among the organisms with identified core exosome complexes, the mode of degradation can differ significantly. In archaeal organisms – which have no known hydrolytic 3'-5' processive exoribonucleases (Koonin et al., 2001) – the exonuclease activity of the core exosome is phosphorolytic and has been attributed to the three

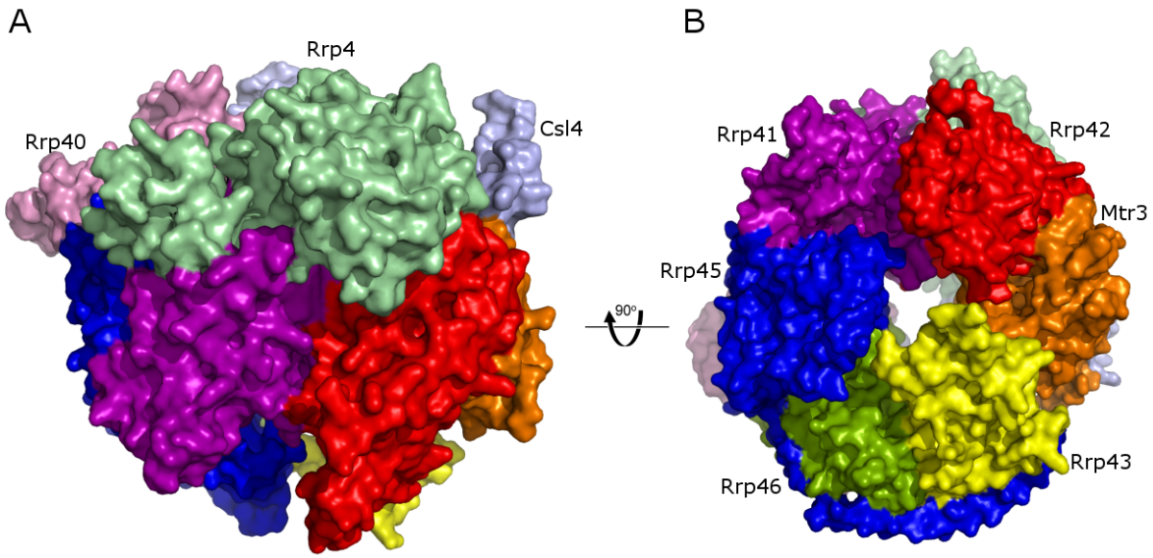

Figure 1. X-ray Crystal Structure of the Human Core Exosome: The human core exosome is composed of nine elements. Panel A is a side view of the ring structure. The top is the RNA entry side and the bottom is the nucleotide release side. Panel A shows the three RNA binding proteins on top upper half of the protein labeled as follows: Rrp40 - Light Purple; Rrp4 - Light Green; Csl4 - Light Blue. Panel B is a 90^{o} rotated view along the horizontal axis of Panel A. Panel B shows a view of the nucleotide exit side of the exosome and is labeled clockwise from the top as follows: Rpr42 - Red; Mtr3 - Orange; Rrp43 - Yellow; Rrp46 - Green; Rrp45 - Blue; Rrp41 - Purple.

Rrp41-like proteins (Lorentzen et al., 2005). The Rrp41-like protomers are not active and require the presence of their cognate Rrp42-like protomer for activity (Lorentzen et al., 2005) which adds biochemical evidence to support the importance of the dimeric interface. In addition, the publication of the crystal structure of the *Pyrococcus abyssi* exosome in complex with RNA shows such an interaction between RNA and the dimeric interface (Navarro et al., 2008).

Eukaryotic organisms have provided the vast majority of the currently available information about the exosome. The core exosome of *Saccharomyces cerevisiae* (*S.cerevisiae*), unlike the archaeal exosome, has no exonuclease activity and requires the presence of an additional protein – termed Rrp44/Dis3 – for activity (Liu et al., 2006). Rrp44/Dis3 is a hydrolytic 3'-5' processive exoribonuclease (Dziembowski et al., 2007), and although it is not constitutively bound to the *S.cerevisiae* exosome, they have been

visualized in complex in cryo-electron microscopy studies (Wang et al., 2007). The Rrp44/Dis3 protein, as the tenth member of the *S.cerevisiae* exosome is the sole source of exonuclease activity *in vivo* (Dziembowski et al., 2007). In addition to its activity as a member of the *S.cerevisiae* exosome, Rrp44/Dis3 is also active as a monomer.

Interestingly, the human core exosome does have exonucleolytic activity, which is in contrast to the inactive *S.cerevisiae* core exosome (Liu et al., 2006). This phosphorolytic 3'-5' processive exoribonuclease activity has been attributed to a single Rrp41-like monomer in the ring complex. Human cells also have an Rrp44/Dis3 protein, which retains all the characteristic activity of the yeast Rrp44/Dis3 protein. However, the human Rrp44/Dis3 protein has not been observed to associate with the human exosome (Liu et al., 2006).

1.3.2 Exonucleolytic RNA Degradation in Prokaryotes

It is a well-established fact that in prokaryotic systems, the message fragments generated by endonucleolytic cleavage are exonucleolytically degraded exclusively in a 3'-5' direction. *E.coli*, which is a model bacterial system used in the study of many cellular processes, has a number of exonucleases; however, only two of these – Polynucleotide phosphorylase (PNPase) and Ribonuclease II (RNase II) – have been implicated in the degradation of bulk RNA (Donovan and Kushner, 1986; Nossal and Singer, 1968). The remaining exonucleases function in the maturation of transfer RNAs (tRNAs) and rRNAs (Cudny and Deutscher, 1980; Deutscher et al., 1988; Kelly and Deutscher, 1992a; Kelly et al., 1992; Li and Deutscher, 1995; Li et al., 1999; Reuven and Deutscher, 1993; Zhang and Deutscher, 1988; Zhou and Deutscher, 1997). PNPase and RNase II are similar in that they are both 3'-5' processive exoribonucleases; however, PNPase degrades RNA

phosphorolytically which generates 5' nucleoside diphosphates, while RNase II degrades RNA hydrolytically, generating 5' nucleoside monophosphates (Deutscher and Reuven, 1991). A study of the degradation products of polyadenylic acid by crude *E.coli* extracts show that over 90% of the nucleotide products are monophosphorylated (Chaney and Boyer, 1972). As a result, RNase II is concluded to be responsible for the degradation of the majority of RNA in *E.coli*.

The upper limit of the degree of processivity of RNase II (the number of nucleotides it can hydrolyze without dissociating) has not yet been established. Rather, the degree of processivity seems to be dictated by either the length of the substrate, or the presence of secondary structure, through which RNase II cannot degrade (Spickler and Mackie, 2000). In both cases, RNase II dissociates from the mRNA molecule and is then free to associate with another mRNA molecule.

There are two particles in *E.coli* that may be involved in the degradation of secondary structure. The first is RNase R (also known as the *vacB* gene product), a protein whose homologues in *Shigella flexneri* and *Aeromonas hydrophila* are known to be involved in virulence (Cheng et al., 1998; Erova et al., 2008; Tobe et al., 1992)**.** RNase II and RNase R are 60% similar (Cheng et al., 1998), suggesting that they are members of the same superfamily (Cheng et al., 1998; Mian, 1997). In addition, RNase II and RNase R are both hydrolytic 3'-5' processive exoribonucleases. However, RNase R has the ability to degrade secondary structure (Cheng and Deutscher, 2002). The second particle that is able to degrade secondary structure is the degradosome, a multienzyme mRNA degradation complex that appears to be structurally unrelated to the eukaryotic exosome. The core protein of the prokaryotic degradosome is RNase E, which contains a putative

scaffolding domain at its C-terminus on which the remaining components of the degradosome are thought to assemble (Vanzo et al., 1998). The other components of the degradosome are enolase, PNPase, and RhlB. The role of enolase, a glycolytic enzyme (Voet and Voet, 2004), in the degradosome is at present not understood. PNPase is the exonucleolytic component of the degradosome, while RhlB, an RNA helicase, is proposed to melt RNA duplexes.

1.3.3 Other Roles for RNase II

Aside from the degradation of mRNA, RNase II appears to play a role in the 3' end maturation of stable RNA such as rRNA and tRNA (Cheng and Deutscher, 2002; Kelly and Deutscher, 1992b; Reuven and Deutscher, 1993). RNase II can generate ribonucleoside 5' monophosphates when incubated with mature 23S, 16S and 5S rRNA as well as tRNA, albeit at a rate that is 3-4 orders of magnitude slower than the rate at which it degrades polyadenylate (Cheng and Deutscher, 2002) – its preferred substrate (Gupta et al., 1977; Singer and Tolbert, 1964; Spahr and Schlessinger, 1963; Spickler and Mackie, 2000). The true difference may not be this large. If there were K_m values available for each of these reactions, it may be apparent why Cheng and Deutscher chose a concentration of rRNA/tRNA that is more than ten times lower than that of polyadenylate. This difference in initial substrate concentration of rRNA/tRNA and polyadenylate may account for some of the difference in apparent activity of RNase II on each substrate. An additional factor that probably influences the difference in rates is the difference in the number of nucleotides hydrolyzed from each substrate. RNase II can completely hydrolyze polyadenylate, which is on the order of several hundred nucleotides in length, while it will not degrade significantly into the mature tRNA and

rRNAs – less than ten nucleotides – (Kelly and Deutscher, 1992b). This inability of RNase II to degrade secondary structure makes it a good candidate for participating in the 3' end maturation of stable RNA. Although RNase II is capable of processing precursor tRNA to the mature 3' CCA end, it is not the preferred enzyme for this process. This is due to the lower fidelity of RNase II in leaving the mature CCA end compared to RNase T or RNase PH (Kelly and Deutscher, 1992b).

A counterintuitive feature of RNase II is its role in the protection of mRNA transcripts from degradation. The polyadenylation of mRNA transcripts has been implicated as a factor which influences gene regulation (Joanny et al., 2007; Marujo et al., 2000). The termination of many bacterial messages is mediated by a process called *Rho*-independent termination (Weaver, 2002). In this process, the formation of a hairpin at the 3' end of a transcript causes the message to be released by the RNA polymerase. In a process whose regulation and purpose is still poorly understood, the 3' end of some mRNA transcripts are polyadenylated (Joanny et al., 2007; Marujo et al., 2000). In some cases, such as in the degradation of the *rpsO* transcript, RNase II removes the polyadenylate tail, but is stopped by the hairpin generated in *Rho*-independent termination (Marujo et al., 2000). The degradation of the polyadenylate tail by RNase II removes the 3' overhang that is proposed to be targeted by the degradosome. This seems to be a mechanism that prevents premature degradation of mRNA (Marujo et al., 2000).

1.4 Activity, Substrates and Inhibitors of RNase II

RNase II is a single-stranded RNA (ssRNA) specific, hydrolytic 3'-5' processive exoribonuclease (Cannistraro and Kennell, 1994, 1999; Nossal and Singer, 1968; Singer and Tolbert, 1964). It requires a divalent cation for activity, and works best with

magnesium ions (Gupta et al., 1977). RNase II retains its activity when manganese substitutes for magnesium, although to a slightly lower extent (Gupta et al., 1977). The chelating agent ethylene diamine tetraacetic acid (EDTA) is an inhibitor of RNase II by virtue of removing all freely available divalent cations from the environment (Gupta et al., 1977). RNase II also requires a monovalent cation for activity. Potassium ions are preferred, and ammonium ions cause RNase II to be slightly less active, while sodium ions have a deleterious effect on activity (Gupta et al., 1977; Kivity-Vogel and Elson, 1968; Singer and Tolbert, 1965). In addition, RNase II requires a pH of between 7 and 8 for optimal activity (Gupta et al., 1977).

RNase II can neither bind nor degrade double-stranded nucleic acids (RNA or DNA) (Singer and Tolbert, 1964; Spickler and Mackie, 2000); however, it can bind nucleic acid containing secondary structure if that nucleic acid has more than six unpaired bases at its 3' end (Cannistraro and Kennell, 1999; Spickler and Mackie, 2000). If the secondary structure is weak enough (approximately 5bp), RNase II is able degrade through that secondary structure (Spickler and Mackie, 2000). It can bind, but not degrade single-stranded DNA (ssDNA), which a competitive inhibitor (Gorelic and Apirion, 1971; Singer and Tolbert, 1965; Spahr, 1964). When presented with secondary structure-free ssRNA substrate, RNase II will bind to the 3' end and processively hydrolyze individual nucleotides until the substrate reaches a length of 4 nucleotides (Barbas et al., 2008; Frazao et al., 2006), at which point RNase II dissociates from the RNA, and cannot further degrade it (Coburn and Mackie, 1996b; Nossal and Singer, 1968; Singer and Tolbert, 1964; Spahr and Schlessinger, 1963). An interesting exception to the substrate specificity of RNase II is its ability to degrade single-stranded DNA/RNA chimeric

oligonucleotides. As long as there are RNA residues at positions 2-6 from the 3' end of the oligomer, RNase II can remove a DNA residue from the 3' end of a nucleic acid chain (Cannistraro and Kennell, 1994). Although the preferred substrate of RNase II is polyadenylic acid, it can degrade RNA independent of sequence (Gupta et al., 1977; Singer and Tolbert, 1964; Spahr and Schlessinger, 1963; Spickler and Mackie, 2000).

Prior to the publication of the X-ray crystal structure of RNase II (Frazao et al., 2006; Zuo et al., 2006), little was known about the relationship between the structure and function of its processivity. One model that has been proposed to describe the processivity of RNase II is the inchworm, or caterpillar, model (Cannistraro and Kennell, 1999). This model proposes that the translocation of an RNA chain into the RNase II active site is a result of a conformational change in either the RNA chain, RNase II itself, or a combination of the two. In examining conformational changes in RNase II, it is assumed that RNase II has an "anchor" region bound at some distance less than 27 bases from the 3' end of the RNA chain (Cannistraro and Kennell, 1999). The "catalytic" region – also with binding capability – catalyzes hydrolysis of nucleotides from the 3'

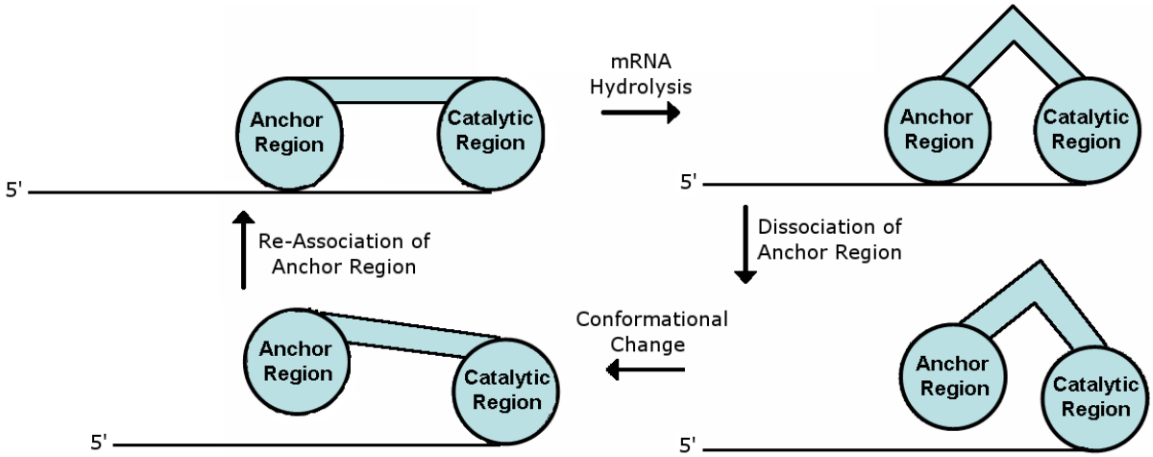

Figure 2. Model of RNase II Processive Degradation: A cartoon of the model of processivity termed the "Caterpiller" model. See text for description.

end of the RNA chain, until it encounters the part of the RNA chain where the anchor region of RNase II is bound. At this point, with the catalytic region still bound, the anchor region dissociates from the RNA and re-associates at a point less than 27 nucleotides 5' to its original position (Figure 2).

1.5 RNase II Structure

Attempts to identify structural domains prior to the publication of the crystal structure relied on sequence homology studies (Amblar et al., 2006). These studies identified two oligonucleotide/oligosaccharide binding (OB) domains; an N-terminal domain homologous to a cold-shock domain, and a C-terminal domain homologous to an S1 domain. Located between these two domains and accounting for the majority of the primary sequence is a novel domain, termed the RNB domain, which contains four conserved sequence motifs (Amblar and Arraiano, 2005a, b). After further analysis, a region of the N-terminal portion of the RNB domain was identified as conserved among homologues but could not be attributed to any known fold (Amblar et al., 2006). When this region is subjected to the 3D-PSSM program-Fold recognition server, a five stranded β-barrel is predicted. Subsequent structural comparisons to known folds found this domain to be structurally similar to the cold-shock domain (Amblar et al., 2006), bringing the number of N-terminal cold-shock domains to two and the number of overall

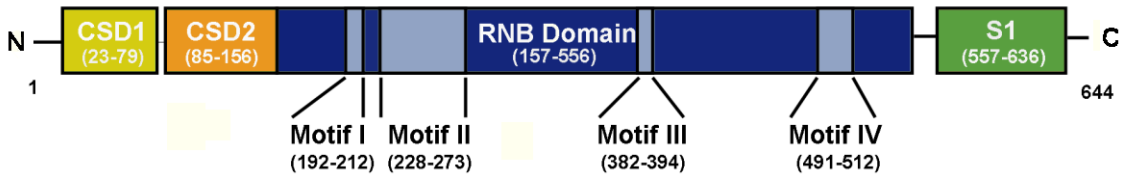

Figure 3. Linear Domain Arrangement of RNase II: A linear representation of RNase II's bioinformatically predicted domains. The OB domains CSD1, CSD2 and S1 flank the central RNB Domain, which contains the four conserved sequence motifs.

OB domains to three. An adaptation of the linear domain arrangement proposed by Amblar *et al.* (2006) is shown in Figure 3.

Shortly after the identification of the second cold-shock domain, the crystal structure of RNase II was solved (Frazao et al., 2006: PDB ID 2IX0, 2IX1; and Zuo et al., 2006: PDB ID 2ID0) and confirmed the presence of the second cold-shock domain (Figure 4A). This structure also provide information used in structure-guided mutational studies (Barbas et al., 2008). The crystal structures (2IX0, 2IX1, 2ID0) confirmed the domain arrangement described above showing two OB domains (CSD1 and CSD2) occupying the N-terminal region, followed by the novel RNB domain, and a third OB domain (S1)

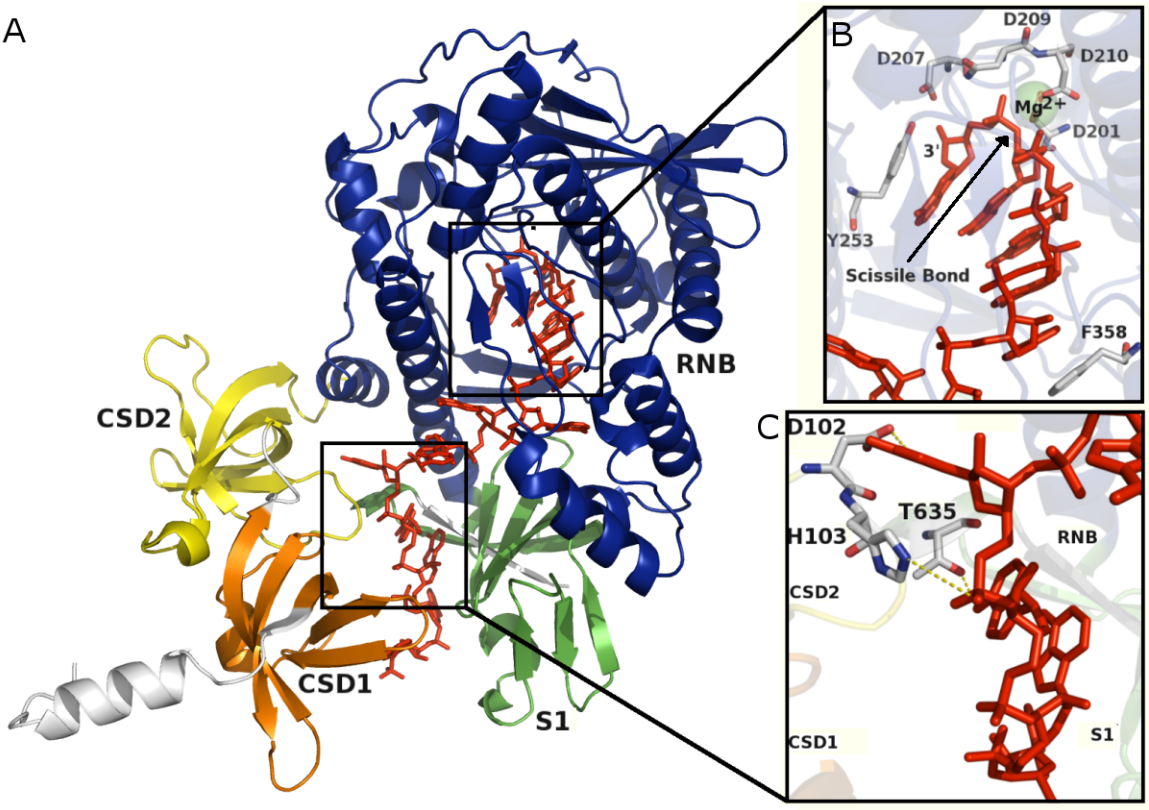

Figure 4. X-ray Crystal Structure of RNase II: Panel A shows a cartoon view of RNA bound RNase II D209N mutant. OB domains CSD1, CSD2 and S1 are coloured orange, yellow and green respectively. The RNB domain is coloured blue, and the RNA is coloured red. Panel B shows a close-up of the catalytic pocket with the catalytic aspartates and the aromatic clamp shown. Panel C shows the RNA bound to the anchor region, made up primarily of residues from the CSD2 and S1 domains.

occupying the C-terminal region of RNase II. Co-published with the RNase II structure is a naturally occurring inactive RNase II mutant, originally identified in an *E.coli* strain with a mutation in the RNase II allele termed *rnb296*. The loss of activity resulting from the *rnb296* mutation was traced to a single nucleotide change of G to A at position 624 which changes residue 209 to an asparagine from an aspartate, (Amblar and Arraiano, 2005a, b). The loss of activity of this mutant – referred to as D209N – is not accompanied by a loss of binding; in fact, the D209N mutant retains the same binding as the active, full-length RNase II. The D209N mutant co-crystallized with a short RNA oligomer, which was undoubtedly a result of its loss of activity (Frazao et al., 2006). This is a remarkable discovery which enabled the visualization of the static enzyme-substrate complex.

1.5.1 Interactions Between RNase II and RNA

The complex of the D209N mutant and the RNA oligomer shows two distinct binding regions between RNase II and RNA (Figure 4B/C). The anchor region is non-catalytic and is made up primarily of interactions between RNA residues 9-13 bases from the 3' end of the RNA chain and residues of the S1 and CSD2 domains. This region appears to be vital for the processivity of RNase II, since oligomers known to be too small to contact both the anchor region and the catalytic domain dissociate following each round of hydrolysis in what is termed distributive degradation (Cannistraro and Kennell, 1994). The catalytic region is situated within the RNB domain and can more accurately be described as a catalytic pocket, which is formed by residues from each of the four conserved sequence motifs (Frazao et al., 2006). It is in this catalytic pocket where the RNA bases are stacked in preparation for hydrolysis (see Figure 6). Steric hindrance

around the entrance to this catalytic pocket precludes access by double-stranded nucleic acids and is thus responsible for single-strand specificity. The residues from the conserved sequence motifs appear to be directly responsible for the correct orientation and cleavage of RNA. In addition they participate in four protein-RNA hydrogen bonding interactions that involve the O2' oxygen of the ribose ring. These interactions account for the specificity of RNase II for RNA over DNA. Approximately half of all hydrogen bonding interactions in the catalytic pocket involve RNA phosphates, indicative of sequence insensitivity.

The active center of the RNase II D209N mutant is incomplete (Figure 5). However, Frazao *et al* (2006) propose a two-metal-ion catalysis mechanism based on the structural homology between D201, D210, D209N and D207 of the RNase II D209N mutant and E109, D132N, E183 and D192 of RNase H, an endonuclease that cleaves the RNA of a

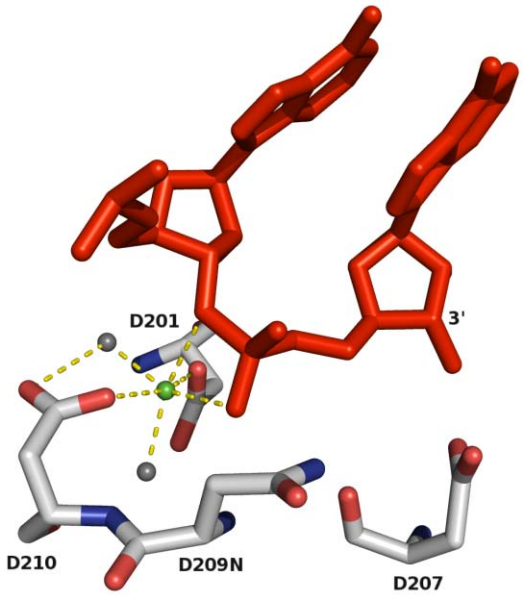

Figure 5. Active Site Interactions Between RNase II and RNA: Interactions between the catalytic aspartates of the RNase II D209N mutants and RNA phosphate mediated by a Magnesium ion (Green sphere) and water molecules (Grey spheres). It is proposed that a second Magnesium ion is co-ordinated by D209 and D207 in order to activate a water for nucleophilic attack on the phosphate.

RNA/DNA duplex which operates via a two-metal-ion catalysis mechanism. In the proposed mechanism, the hypothesized magnesium ion, which is co-ordinated by the side-chains of D207 and D209, activates a water which then acts as a nucleophile and attacks the phosphorus of the leaving nucleotide in an S_N2 type reaction, with the O3' of the penultimate nucleotide as the leaving group. The structure also shows an aromatic clamp (Figure 6), in which five RNA bases at the 3' end of the RNA chain are base-stacked between Y253 at the 3' end and F358 at the 5' end. This aromatic clamp has been shown to be vital for binding in the catalytic pocket. Mutational studies have shown that both Y253 and F358 are equally interesting for binding in the catalytic pocket. The more highly conserved of the two, Y253, seems to be implicated in catalytic site binding. Mutation to an alanine results in an increase in size of the smallest observed end product from 4 nucleotides to 10 (Barbas et al., 2008). Barbas *et al* (2008) propose

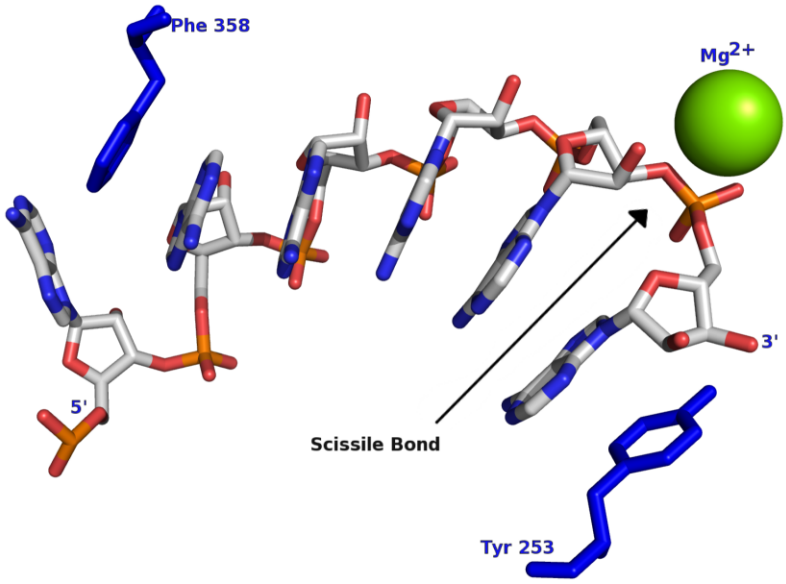

Figure 6. Base-Stacking Interaction of Nucleotide Bases in the Catalytic Pocket: A close-up view of six residues at 3' end of RNA chain bound to RNase II. The five residues at the 3' end of the chain are base-stacked and clamped between Tyr253 and Phe358. The sixth residue from the 3' end does not participate in base-stacking interactions with its neighbouring bases or Phe358.

that this is due to the inability of the catalytic pocket of the Y253A mutant to bind substrates between 5 and 10 nucleotides in length that wild-type RNase II is able to degrade. Additionally, molecular dynamics simulations suggest that Y253 may be involved in a potential mechanism for removal of the cleaved nucleotide from the active site (Barbas et al., 2008). When the outgoing nucleotide residue shifts from an *anti* to *syn* conformation, the base-stacking interaction between the outgoing and penultimate nucleotide is eliminated. The Y253 side-chain maintains its base-stacking interaction with the outgoing nucleotide, and appears to pull it from the active site using base-stacking interactions. The importance of Y253 is supported by the structural conservation of tyrosine in the *S.cerevisiae* Rrp44/Dis3 protein (Lorentzen et al., 2008). This is perhaps a more plausible explanation for the removal of the cleaved nucleotide than that proposed in the original report of the RNase II structure. The original hypothesis proposes that the E542 side-chain forms hydrogen bonds with N1 and N6 of the outgoing adenylate (Frazao et al., 2006). This mechanism is inconsistent with the sequence insensitivity of RNase II, as these interactions would not be present in other nucleotide bases, although it would account for the preference for polyadenylate. Experimental analysis is required to reveal the true mechanism of nucleotide removal from the active site.

The 5' end of the aromatic clamp, F358, appears to have a role in the advancement of the RNA chain towards the active site (Barbas et al., 2008). The F358A mutant generates a major breakdown product that is one nucleotide larger than the wild-type protein generates. This experimental evidence shows that the F358A mutant is impaired in its ability to move the substrate into the position required for the generation of the 4

nucleotide end product. This hypothesis is supported by Barbas *et al.* (2008) with molecular dynamics simulations of the D209N mutant in complex with the RNA oligomer. The crystal structure shows F358 base-stacking with the fifth nucleotide from the 3' end of the RNA chain. However, the simulations show F358 rotating away from its position in the crystal structure. Barbas *et al* (2008) interpret this movement as the initiation of a propeller-like movement, which pushes the substrate into the catalytic pocket. F358 is not well conserved and is notably absent in the orthologous Rrp44/Dis3 and paralogous RNase R (Lorentzen et al., 2008). Based on the conservation of F358, this type of advancement mechanism, should it turn out to be an accurate representation of the *in vivo* function, would seem to be unique to RNase II.

1.5.2 Interactions Between RNA and the Active Center Aspartates of RNase II

Sequence analysis of RNase II homologues performed by Barbas *et al* (2008) show that there are four aspartate residues (201, 207, 209, 210) that are completely conserved among the chosen homologues. In a more extensive analysis of RNase II homologues, D207, while highly conserved, does not share the same degree of virtually universal conservation as D201, D209 and D210. Interestingly, the majority of residues that differ from aspartate at these positions are glutamates, an amino acid with the same functional group.

Although D207 is highly conserved, it is not functionally as important as the other aspartate residues (Barbas et al., 2008), which is suggested by its slightly lower conservation compared to D201, D109 and D210. This is supported by mutational studies, in which aspartate 207 is mutated to asparagine, resulting in a drop to 12% activity, a significant drop in activity, but not nearly as significant as the drop in activity

seen when the other aspartates are mutated. Additionally, despite the apparent importance of its side chain in the crystal structure and its high level of conservation, molecular dynamics simulations of the D209N mutant with bound RNA oligomer, show that the side chain of D207 moves away from the catalytic center, causing its main chain oxygen to reposition so as to co-ordinate the active site magnesium ion.

The active site depicted in the crystal structure of the RNase II D209N mutant shows a magnesium ion co-ordinated by the oxygens of two waters, along with the side chains of D201 and D210 (Figure 5) (Frazao et al., 2006). Mutation of either of these two aspartates to asparagines does not completely abolish the activity of RNase II, but it does reduce the activity to 0.2% and 0.3% of the wild-type activity respectively (Barbas et al., 2008). The change in binding affinity of these mutants is only 2-fold when binding to a 25 residue RNA oligomer, indicating that these mutations do not affect overall binding. Rather, Barbas *et al.* (2008) propose that these residues are involved in catalytic activity. In addition to the drop in activity, each of these mutations generate larger end products of 10 to 11 nucleotides from approximately 5 generated by wild-type RNase II. This product corresponds to the smallest RNA oligomer able to contact both the catalytic pocket and anchor region of RNase II. This is interpreted by Barbas *et al.* (2008) that in the absence of binding between RNA and the anchor region, the catalytic pocket is unable to maintain its grasp on the RNA, and as a result releases the substrate. So, in addition to a potential involvement in catalytic activity, these residues confer binding ability to the catalytic pocket. However, Barbas *et al.* (2008) do not consider the possibility that the loss of activity in the D201A and D210A mutants may simply be a result of the decreased affinity of the catalytic pocket for RNA, and that the relatively

unchanged overall binding may be a result of the strong binding in the anchor region masking a drastically reduced binding affinity in the catalytic pocket.

The mutation that causes the greatest disruption of RNase II activity involves another aspartate residue. The mutation of residue 209 from an aspartate to an asparagine completely abolishes the ability of RNase II to hydrolyze RNA (Amblar and Arraiano, 2005a, b). As noted earlier, this residue is thought to co-ordinate the magnesium that activates the nucleophilic water. In spite of this proposed catalytic importance, this mutation does not affect overall binding. Although the crystal structure shows RNA in the catalytic pocket of the D209N mutant, the possibility that unchanged anchor region binding is masking a decrease in the binding of RNA to the catalytic pocket cannot be eliminated.

1.5.3 Structure of Homologous Proteins

As RNase II is been proposed to be the model protein for the RNR family of exoribonucleases (Mian, 1997) two homologous proteins – RNase R and Rrp44/Dis3 – have been computationally modeled based on the structure of RNase II (Barbas et al., 2008). However, the recently published crystal structure of the *S.cerevisiae* RNase II homologue, Rrp44/Dis3, shows a distinct difference in the arrangements of the oligonucleotide binding domains (Lorentzen et al., 2008). This difference is in spite of a common linear domain arrangement, 8-14% sequence identity and individual domain superposition of 70% of α-carbons between 2.2 and 2.8Å (Lorentzen et al., 2008). The authors of the paper suggest that the difference in domain arrangements enable RNase R and Rrp44/Dis3 to degrade secondary structures.

1.6 Project Overview

In general terms, the goal of this project is to study the structure and function of RNase II in order to shed light upon mRNA degradation mechanisms. More specifically, the project is aimed at quantifying the structural dynamics of RNase II in order to understand its processive catalytic mechanism and function.

Relatively few experimental techniques can directly quantify molecular movements. One such method is called Fluorescent Resonance Energy Transfer (FRET). FRET efficiency can be used to measure separation distances between dye pairs within a single molecule or complex. When measuring the distance between dye pairs in a complex, FRET signals can provide the basis for binding assays with little interfering background signal. Site-directed mutagenesis also provides the ability to label specific residues for separation distances within a single molecule.

The strategic placement of dyes on the molecular surface of a protein that are predicted to move relative to each other allows for distance information to be gathered through the measured FRET efficiency. This provides a method of detecting events where the donor and acceptor fluorophores interact with each other over a distance on the order of tens of angstroms. Although it is possible to systematically label pairs of residues throughout the primary sequence of RNase II, structural information expedites the process of identifying suitable residues for labeling.

At the beginning of this project, RNase II was structurally uncharacterized. Only two regions of the primary sequence were known to be homologous to characterized structural domains. In the absence of high resolution structural information, a domain map is sufficient for identifying potential targets for fluorescent labeling. In order to

generate a domain map, a series of C-terminal deletion mutants were generated based on predicted domain boundaries and assayed for activity. The publication of the high resolution structure (Frazao et al., 2006; Zuo et al., 2006) at the midpoint of the project helped to explain the behaviour of the mutants, and provided the starting point for fluorescent studies. The presence of a crystal structure in which all the domains are defined allows for a much more accurate labeling of domains.

Since the fluorescent labeling of RNase II can effect its activity, a significant portion of the research project is identifying suitable fluorescent labels for subsequent experimentation. In order to confirm and complement initial fluorescent binding studies, binding was measured using a gel-shift assay, as well as with Isothermal Titration Calorimetry (ITC). ITC has the advantage of providing information that cannot be obtained in fluorescent binding experiments, such as the contribution of enthalpy and entropy to substrate binding.

Chapter 2: Materials and Methods

2.1 Buffers and Reagents

Acrylamide Solution (30% (w/v))

29g	Acrylamide
1g	Bis-acrylamide

Dilute to 100mL with deionized H_2O

Acrylamide Solution (20% (w/v))

19g	Acrylamide
1g	Bis-acrylamide

Dilute to 100mL with deionized H_2O

SDS-PAGE Resolving Gel Premix (12% (w/v))

4.0mL	30% Acrylamide Solution
2.5mL	Tris-HCl (1.5M pH8.8)
0.1mL	SDS (10% (w/v))
3.4mL	Deionized H_2O

SDS-PAGE Stacking Gel Premix (5% (w/v))

0.65mL	30% Acrylamide Solution
1.25mL	Tris-HCl (0.5M pH6.8)
0.05mL	SDS (10% (w/v))
3.05mL	Deionized H_2O

Tris-Glycine Buffer (1x)

14.4g	Tris
3.0g	Glycine
1.0g	SDS

Dilute to 1L with deionized H_2O

SDS-PAGE Sample Reducing Buffer (2x)

1.80mL	Glycerol (100%)
2.16mL	Tris-HCl (0.5M pH6.8)
4.00mL	SDS (10% (w/v))
1.00mL	β-mercaptoethanol
1.00mL	Bromophenol blue (0.1% (w/v))

SDS-PAGE Staining Solution

40% (v/v)	Methanol
10% (v/v)	Acetic acid
50% (v/v)	Deionized H_2O
0.25% (w/v)	Coomassie brilliant Blue

SDS-PAGE Destaining Solution

40% (v/v)	Methanol
10% (v/v)	Acetic acid
50% (v/v)	Deionized H_2O

TAE Buffer (50x)

242g	Tris
57.1mL	Glacial acetic acid
100mL	EDTA (0.5M pH8.0)

Dilute to 1L with deionized H_2O

TBE Buffer (5x)

54.0g	Tris
27.5g	Boric acid
20mL	EDTA (0.5M pH8.0)

Dilute to 1L with deionized H_2O

Agarose Gel Loading Buffer (Blue Juice)

1.6mL	EDTA (0.25M pH8.0)
1.0mL	Sarkosyl (20% (w/v))
10mg	Bromophenol blue
15% (v/v)	Glycerol
13.4mL	Deionized H_2O

Urea/Acrylamide Solution (15% (w/v))

4.8g	Urea
5.625mL	20% Acrylamide Solution
200.0µL	TAE (50x)
40.0µL	EDTA (0.5M pH8.0)
1.875mL	Deionized H_2O

Urea PAGE Loading Buffer

700µL	8M Urea
20% (v/v)	Glycerol
100µL	Bromophenol blue (0.1% (w/v))

Urea PAGE Staining Solution

0.5% (v/v) Ethidium bromide in deionized H_20

Urea PAGE Destaining Solution

Deionized H_20

Native PAGE Solution (5% (w/v))

2.5mL	20% Acrylamide Solution
1.0mL	TBE (5x)
6.5mL	Deionized H_2O

Native PAGE Loading Buffer

100µL	TBE (5x)
20% (v/v)	Glycerol
100µL	Bromophenol blue (0.1% (w/v))

Silver Stain Solution 1

0.2% (w/v)	$AgNO_3$

Silver Stain Solution 2

0.36% (w/v)	NaOH
0.9% (w/v)	NH_4OH

Silver Stain Developing Solution

0.005% (w/v)	Citric acid
0.02% (w/v)	Formaldehyde

RNB Buffer

1mM	$MgCl_2$
100mM	KCl
20mM	Tris-HCl (pH 7.5)
1mM	DTT
5% (v/v)	Glycerol

Buffer A

1mM	$MgCl_2$
100mM	KCl
20mM	Tris-HCl (pH 7.5)
1mM	DTT
5% (v/v)	Glycerol
25mM	Imidazole (pH8.0)

Buffer B

1mM	$MgCl_2$
100mM	KCl
20mM	Tris-HCl (pH 7.5)
1mM	DTT
5% (v/v)	Glycerol
250mM	Imidazole (pH8.0)

Equilibration Buffer

1mM	$MgCl_2$
100mM	KCl
20mM	Tris-HCl (pH 7.5)
10mM	β-mercaptoethanol

Labeling Buffer

1mM	$MgCl_2$
100mM	KCl
20mM	Tris-HCl (pH 7.5)
5% (v/v)	Glycerol

Elution Buffer

1mM	$MgCl_2$
100mM	KCl
20mM	Tris-HCl (pH 7.5)
5% (v/v)	Glycerol
250mM	Imidazole (pH8.0)

Fluorescein Solution

12.5mg 5-IAF in 500µL DMSO

2.2 Detection Techniques

2.2.1 Sodium Dodecyl Sulfate Polyacrylamide Gel Electrophoresis (SDS-PAGE)

SDS-PAGE followed the method of Laemmli (1970). Gels with a 12% resolving gel and a 5% stacking gel were assembled into a Mini-Protean 3 gel apparatus (Biorad, Hercules, CA, USA). The inner and outer reservoirs were filled with 1x Tris-glycine buffer and protein samples were mixed with an equal volume of 2x SDS-PAGE sample reducing buffer. A voltage of 30V/cm was applied to the gel for approximately 45min at 293K. Gels were immersed in SDS-PAGE staining solution and agitated for approximately 10min at 293K, then transferred to an SDS-PAGE destaining solution and agitated for approximately 20min at 293K.

2.2.2 Agarose Electrophoresis

Agarose gels were made by heating 0.32g of Agarose B (Bio-Basic; Markham, ON, Canada) in 40mL of 1x TAE buffer to make a 0.8% (w/v) agarose gel. Once cooled to approximately 320K, but prior to casting, ethidium bromide was added to a final concentration of 0.5% (v/v). The cooled and solidified agarose gel was placed in a Mini-Sub Cell GT Cell (Biorad) and immersed in 1x TAE. DNA samples were mixed in an equal volume of agarose gel loading buffer and loaded into the agarose gel. A voltage of 6V/cm was applied to the gel for approximately 60min at 293K. The gels were placed on a transilluminator (VWR International; West Chester, PA, USA) so that bands could be visualized by ultraviolet illumination at 302nm.

2.2.3 Urea PAGE

900mL of 1x TAE buffer was heated to approximately 320K prior to use. A Mini-Protean 3 gel apparatus (Biorad) was assembled with polymerized

Urea/Acrylamide (15% acrylamide in 8M urea) gel in place. The inner and outer reservoirs of the gel apparatus were filled with the pre-heated 1x TAE buffer, and run without samples at 40V/cm for 5min in order to pre-heat the gel. Samples were mixed in an equal volume of urea gel loading buffer and heated at 368K for 5min prior to loading. Once samples were loaded, a voltage of 40V/cm was applied to the gel for approximately 30min at 293K. Gels were immersed in a 0.5% solution of ethidium bromide and agitated for 20min. Following immersion in ethidium bromide, gels were placed on transilluminator so that bands could be visualized at 302nm and photographs taken for densitometric analysis with IMAGEJ software (Abramoff et al., 2004).

2.2.4 Native PAGE

A Mini-Protean 3 gel apparatus (Biorad) was assembled with polymerized 5% native PAG in place. The inner and outer reservoirs were filled with 0.5x TBE. Samples were mixed in an equal volume of native PAGE loading buffer and loaded into wells. A constant current of 20mA was applied to the gels for 30min at 277K. Protein bands were visualized using the silver staining protocol, as follows: Gels were soaked in 200mL of 7% (v/v) acetic acid for 5min prior to being soaked in 200mL of 50% (v/v) methanol for 40min, with an exchange of methanol solution after 20min. Gels were rinsed with 200mL deionized H_2O for 20min with an exchange of deionized H_2O after 10min. Gels were immersed in staining solution (silver stain solution 1 added dropwise to silver stain solution 2 and brought up to a volume of 100mL with deionized H_2O) for 15min. Gels were then rinsed in 200mL deionized H_2O for 10min with an exchange at 5min. Gels were then immersed in silver stain developing solution until bands were visible.

Developing reactions were quenched by immersion in 3 changes of 200mL deionized H_2O.

2.2.5 Spectroscopic Quantification of Protein Under Denaturing Conditions

Protein was denatured in 6M guanidine HCl and its absorbance was measured at 280nm (Layne, 1957; Stoschek, 1990), except when measuring 5-IAF covalently bound to RNBec_N22, where the absorbance was measured at 492nm. Concentration values were calculated using the Beer Lambert equation. Extinction coefficients were obtained using the ExPASy server's ProtParam tool (Gasteiger et al., 2005), except for 5-IAF (Kapakos and Steinberg, 1982); all are listed in table 1.

Table 1: Extinction coefficient used in quantification of proteins and 5-IAF

Molecule Measured	Extinction coefficient ($M^{-1}cm^{-1}$)
RNBec_N22	ε_{280} = 66000
RNBst_N22	ε_{280} = 68000
RNBec_N22_c60	ε_{280} = 65000
RNBec_N22_c170	ε_{280} = 49000
RNBec_N22*5IAF	ε_{492} = 77000

2.2.6 Spectroscopic Quantification of Protein Using the Bradford Assay

800µL of deionized H_2O was mixed with 200µL of 1x Bradford reagent (BioBasic) (Bradford, 1976; Stoschek, 1990) and incubated at room temperature for 5min, then the absorbance was measured at 595nm to obtain a zero reading. A standard curve was constructed by measuring A_{595} as described above, replacing 800µL of deionized water with 800µL of 2-10µg/mL Bovine Serum Albumin standard (Pierce Biotechnology; Rockford, IL, USA). The A_{595} of protein samples were measured as above, and compared to the standard curve to determine their concentration.

2.3 Generation of Recombinant RNase II Protein and its Variants

2.3.1 Protein Purification

All proteins were obtained using the following conditions. *Escherichia coli* BL21 (DE3) cells from glycerol stocks containing plasmids summarized in table 2 were streaked onto an LB agar plate containing 50µg/mL of the antibiotic Kanamycin and allowed to grow at 310K overnight. 3mL of LB liquid media containing 50µg/mL of Kanamycin was inoculated with cells from a single colony and allowed to grow at 310K overnight with agitation. 1L of LB liquid media containing 50µg/mL of Kanamycin was inoculated with 1mL of the resulting culture and incubated at 310K with agitation. Overexpression was initiated by the addition of 0.5mM IPTG when OD_{600} reached 0.6. Cells were allowed to overexpress as described in table 3.

Cells were pelleted by centrifugation at 5500xg in a TS-5.1-500 bucket rotor (Beckman Coulter; Fullerton, CA, USA) with an Allegra 25R benchtop centrifuge for 20min at 277K and resulting cell pellets were resuspended in cold buffer A. Cells were lysed by sonication using a Sonic Dismembrator Model 100 (Fisher Scientific), with three 45s bursts, alternated with 30s pauses on ice. The cellular debris was pelleted at 21100xg in a TA-14-50 fixed angle rotor (Beckman Coulter) for 60min at 277K. The supernatant was applied to a NiNTA agarose LPLC (Biorad) column pre-charged with buffer A. Once A_{280} measurements had reached baseline, the protein was removed from the column by step elution with buffer B. The protein sample was then concentrated to approximately 1mL using an Amicon 30kDa molecular weight cut-off centrifugal spin cell (Millipore; Billerica, MA, USA). The protein sample was then further purified on an SEC 200 column (Pharmacia Biotech; Piscataway, NJ, USA) using a BioLogic DuoFlow HPLC

Table 2: Plasmids coding for RNase II and its variants. Bold letters in 'Primers Used" column indicate residues targeted for mutation.

Plasmid	Source	Gene product	Antibiotic Resistance	Primers Used
pET28b(+):: NheI: *RNBec_ N22*	*rnb* gene was PCR amplified from pGC100 (a gift (Coburn and Mackie, 1996b)) and inserted into the NheI site of the pET28b(+) multiple cloning site.	RNBec_ N22	Kanamycin	F: 5'-GTC TAG CTA GCA TTA GTA CTG AAC CCG GTC C-3' R: 5'-ATG ATG CTA GCT TAC GGG CGC GCA ATA ATA CT-3'
pET28b(+):: NheI: *RNBec_ c60*	Modified inverse PCR mutagenesis of pET28b(+)::NheI:*RNBec_N22*	RNBec_ N22_ c60	Kanamycin	F: 5'-TAA TGG TGG ACA GCA AAT GGG TC -3' R: 5'-GGC TTT GTC TTT GAG GAA GCG TG-3'
pET28b(+):: NheI: *RNBec_ c170*	Modified inverse PCR mutagenesis of pET28b(+):: NheI:*RNBec_N22*	RNBec_ N22_ c170	Kanamycin	F: 5'-TAA TGG TGG ACA GCA AAT GGG TC -3' R:5'-CAA ATG ACT GGA AGC GAC GAA TG -3'
pET28b(+):: NheI: *RNBec_ N22_ D209N*	Quikchange mutagenesis of pET28b(+)::NheI: *RNBec_N22*	RNBec_ N22_ D209N	Kanamycin	F: 5'-GCG AAA AGG GCG T**T**A TCC ATA TCT TC**A** GT**A** CTG GC -3' R: 5'-GCC AG**T** AC**T** GAA GAT ATG GAT **A**AC GCC CTT TTC GC -3'
pET28b(+):: NheI:*RNBst_N22*	*rnb* gene PCR amplified from BAC 4027 of *Salmonella enterica* serovar Typhimurium LT2 obtained from the SGSC and inserted into the NheI site of the pET28b(+) multiple cloning site.	RNBst_ N22	Kanamycin	F: 5'-ATA GCT AGC ATG TTT CAG GAC AAC CCG CTG-3' R: 5'-AAA GCT AGC TTG AGT GAG CTA AGC GTG G-3'

Table 3: Overexpression conditions of *Escherichia coli* BL21(DE3) cells.

Gene Product	Overexpression conditions
RNBec_N22	Overnight (~16h) at 310K
RNBst_N22	Overnight (~16h) at 310K
RNBec_c60	3h at 303K
RNBec_c170	3h at 303K

(Biorad). The sample was again concentrated to obtain a concentration in excess of 100μM (10mg/mL; typically about 500μL). In addition, the sample was quantified using the Bradford and denaturing methods, brought to 20% glycerol, and stored in small aliquots at 193K until needed.

2.3.2 Fluorescent Labeling of RNase II with 5-IAF

2.5mL of a 50% NiNTA sepharose was transferred to a 15mL conical tube. The resin was pelleted by spinning the slurry at 500xg in a TS-5.1-500 bucket rotor for 5min at 277K. The resin was then equilibrated by washing three times with 10mL of equilibration buffer. Following equilibration, the resin was pelleted as described above to remove excess buffer. Once equilibrated, 175nmol of RNBec_N22 and 6mL of equilibration buffer were added to the resin. The resin was resuspended and incubated for 5h at 277K with occasional agitation. Following incubation the resin was pelleted by centrifugation as described above. The resin was then equilibrated with labeling buffer by washing five times with 10mL volumes. The supernatant from all samples was retained and analyzed with SDS-PAGE. After the final wash with labeling buffer, the resin was resuspended in 4mL of labeling buffer. Following resuspension, 3.6μmol of 5-IAF (112μL of 30mM 5-IAF in DMSO) was added dropwise to the resin for a 20-fold excess of dye over protein. The resin was incubated for 3h at 293K with agitation. Following incubation, the resin was washed with labeling buffer until supernatant was colourless. The resin was pelleted by centrifugation as described above, the supernatant was removed, and 1.5mL elution buffer was added to the resin which was then resuspended and incubated on ice for 30min. The resin was pelleted as described above and the supernatant – containing labeled RNase II – was removed and retained in light proof container. Elutions were

repeated until the supernatant was colourless. Imidazole was removed from sample by buffer exchange using an Amicon 30kDa molecular weight cut-off centrifugal spin cell (Millipore) as follows. 10mL of sample was added to an Amicon 30kDa molecular weight cut-off centrifugal spin cell and centrifuged at 3405xg in an Allegra 25R benchtop centrifuge using a TS-5.1-500 bucket rotor until the sample volume was reduced to approximately 1mL, with occasional stops to mix the sample in order to avoid precipitation. Once the volume reached 1mL, 9mL of RNB buffer was added and centrifugation was repeated. This procedure was repeated until a 1:1000 dilution of imidazole was achieved. The sample was concentrated to a final volume of 2mL, removed to microcentrifuge tubes and subsequently spun at maximum speed (>10000xg) in an Eppendorf 5415C microcentrifuge (Eppendorf; Westbury, NY, USA) at 277K for 10min to pellet any precipitate. The protein and 5-IAF concentrations were determined independently by denaturing absorbance spectroscopy at 280nm and 492nm respectively. Glycerol was added to a final concentration of 20%, and samples were aliquoted into small volumes and stored at 193K for future use.

2.3.3 Site-directed Mutagenesis to Generate RNase II D209N mutant

The Quikchange mutagenesis protocol from Stratagene (La Jolla, CA, USA) was followed to generate an inactive mutant by mutating aspartate 209 to an asparagine. The template DNA used was pET28b(+)::NheI:*RNBec_N22*, obtained by purification from *E.coli* DH5α cells. Primers are described in table 2 and introduce three nucleotide changes. One of the nucleotide changes results in an asparagine residue to be coded rather than an aspartate. The other two changes are silent mutations, not affecting the

protein primary sequence, but introducing a novel endonuclease cleavage site. The PCR reaction and cycling conditions are described in tables 4 and 5.

Following amplification, the parental DNA was removed by digestion with DpnI endonuclease for 3h at 310K. The amplification products were transformed into *Escherichia coli* (DH5α) cells. 3mL of LB liquid media containing 50µg/mL of Kanamycin was inoculated with cells from the resulting single colonies and incubated overnight at 310K with agitation. Once the gene was sequenced to confirm mutations, cells were stored at 193K in 30% glycerol for future use. Plasmid DNA containing the *RNBec_N22_D209N* gene from *E.coli* DH5α was transformed into *E.coli* BL21(DE3) cells and tested for overexpression. The BL21(DE3) cells that overexpress RNBec_N22_D209N were also stored at 193K in 30% glycerol.

Table 4: Reaction conditions for Quikchange mutagenesis generating RNBec_N22_D209N mutant

Reaction Component	Volume (µL)
Template DNA (50ng/µL)	20.0
Deionized H_2O	12.8
Forward Primer (5µM)	5.0
Reverse Primer (5µM)	5.0
dNTP (10mM)	1.0
$MgSO_4$ (100mM)	1.0
10x ThermoPol Buffer	5.0
RNA Polymerase	0.2

Table 5: Thermocycler settings for Quikchange mutagenesis generating RNBec_N22_D209N mutant

Action	Temperature (K)	Time (s)
Initial Denature	368	300
Denature	368	30
Anneal	333	30
Extend	345	480
Final Extend	345	300
Storage	277	Indefinite

2.4 RNA Degradation Assay

A 16μL reaction mix was prepared containing 30nM MS2 RNA in RNB buffer. Various concentrations of RNBec_N22 (0.5-5μM) were added to the reaction mix to initiate the assay. A time zero sample was immediately removed and quenched with an equal volume of Urea Gel Loading Buffer. The reaction mix was incubated at 310K, with 2μL aliquots drawn at 10min intervals over a period of 60min. Aliquots were pipetted into an equal volume of Urea Gel Loading Buffer and stored at 293K prior to analysis with Urea PAGE. Immediately following the removal of the final aliquot, all samples were heated at 368K for 5min, after which they were immediately loaded on the Urea/Acrylamide gel for analysis.

2.5 Measurement of Binding by Fluorescence

All fluorescence measurements were obtained from a Cary Eclipse fluorimeter (Varian; Palo Alto, CA, USA). In order to prevent adsorption of protein to the cuvette wall, the cuvette walls were blocked by adding 300μL of 10mg/mL BSA to the 3mm x 3mm cuvette and incubating for 20min at 293K. Measurements were taken in triplicate at slow speed (120nm/min; 1nm increments) with 5nm excitation and emission slit widths at 293K after a 2min equilibration period following injection of titrant. All data sets were corrected for dilution values and background fluorescence. Fluorescence data points were obtained by averaging data from fluorescent emission across 10nm, centered on the fluorescence emission maxima. This data was plotted as a function of titrant concentration. Dissociation rate constants were obtained by fitting a curve to the data (see Appendix A for equation) (Goodrich and Kugel, 2007).

Table 6: A summary of fluorophores used in fluorescent binding experiments and their maximum absorbance wavelengths and measured emission wavelengths.

Experiment	**Type of Experiment**	**Excited Fluorophore** (Absorbance Maxima)	**Emitting Fluorophore(s)** (Wavelengths measured)
1	Direct Excitation	Tryptophan (280nm)	Tryptophan (280-500nm)
2	Direct Excitation	5-IAF (492nm)	5-IAF (502-600nm)
3	Direct Excitation	2-AP (310nm)	2-AP (325-500nm)
4	FRET	Tryptophan (280nm)	Tryptophan/5-IAF (280-600nm)

The excitation and measured emission wavelengths for different experiments are summarized in table 6.

2.5.1 Measurement of Intrinsic Protein Fluorescence

After blocking, approximately 290µL of RNB buffer was added to the cuvette. RNBec_N22 was added to the cuvette to give a final concentration of 500nM and excited according to table 6, experiment 1 to measure the background fluorescence. A total of 11 2µL individual injections of an 1892µM dA(30) solution were added to the RNBec_N22 sample; each addition of dA(30) increased its concentration in the sample by approximately 12µM, to a final concentration of approximately 120µM. After each addition, the intrinsic tryptophans of RNBec_N22 were directly excited and the resulting tryptophan fluorescence was measured according to table 6, experiment 1.

2.5.2 Measurement of Non-Natural Protein Fluorescence

After blocking, approximately 290µL of RNB buffer was added to the cuvette. RNBec_N22*5IAF was added to the cuvette to give a final concentration of 500nM and excited according to table 6, experiment 2 to measure the background fluorescence. A total of 6 2µL individual injections of an 1892µM dA(30) solution were added to the RNBec_N22 sample; each addition of dA(30) increased its concentration in the sample

by approximately 12μM, to a final concentration of approximately 70μM. After each addition, the fluorescein molecules bound to RNase II were directly excited and fluorescein's resulting fluorescence was measured according to table 6, experiment 2.

2.5.3 Measurement of Non-Natural Ligand Fluorescence

2.5.3.1 Titration of Fluorescent Ligand into Protein

After blocking, approximately 295μl of RNB buffer was added to the cuvette. RNBec_N22 was added to give a final concentration of 1.5μM or 5.0μM and excited according to table 6, experiment 3 to measure the background fluorescence. A total of 10 2μL individual injections of a 500μM dA(30)-2-AP solution was added to the RNBec_N22 sample; each addition of dA(30)-2-AP solution increased its concentration in the sample by approximately 3μM, to a final concentration of approximately 30μM. After each addition, the 2AP residue in dA(30)-2-AP was excited and its resulting fluorescence was measured according to table 6, experiment 3.

2.5.3.2 Titration of Protein into Fluorescent Ligand

After blocking, approximately 275μL of RNB buffer was added to the cuvette. dA(30)-2-AP was added to a final concentration of 5μM and excited according to table 6, experiment 3 to measure the background fluorescence. A total of 36 1μL individual injections of a 625μM RNBec_N22 solution was added to the dA(30)-2-AP sample; each addition of RNBec_N22 increased its concentration in the sample by approximately 4μM, to a final concentration of approximately 70μM. After each addition, the 2AP residue in dA(30)-2-AP was excited and its resulting fluorescence was measured according to table 6, experiment 3.

2.5.3.3 Protection of Ligand Fluorescence from Quenching

In a protection assay, dA(30)-2-AP was incubated in the presence of acrylamide, a quenching agent. After blocking, 242μM of RNB buffer was added to the cuvette. dA(30)-2-AP was added to a final concentration of approximately 2μM and its unquenched fluorescence measured according to table 6, experiment 3. Acrylamide was then added to a final concentration of approximately 300mM acrylamide and the quenched 2-AP fluorophore was excited according to table 6, experiment 3 to establish a baseline measurement. A total of 13 2μL individual injections of a 266μM RNBec_N22 solution was added to the dA(30)-2-AP sample; each addition of RNBec_N22 increased its concentration in the sample by approximately 2μM, to a final concentration of approximately 20μM. After each addition, the 2AP residue in dA(30)-2-AP was excited and its resulting fluorescence was measured according to table 6, experiment 3.

2.5.4 Measurement of Fluorescence Resonance Energy Transfer (FRET)

After blocking, approximately 290μL of RNB buffer was added to the cuvette. RNBec_N22*5IAF was added to a final concentration of 500nM and excited according to table 6, experiment 4 to establish a baseline measurement. A total of 9 2μL individual injections of an 1892μM dA(30) solution were added to the RNBec_N22 sample; each addition of dA(30) increased the concentration of dA(30) in the sample by approximately 12μM, to a final concentration of approximately 95μM. After each addition, the intrinsic tryptophan of RNase II was excited, and the resulting fluorescence from the intrinsic tryptophans as well as from the bound 5-IAF molecules were measured according to table 6, experiment 4.

2.6 Measurement of Binding by Isothermal Titration Calorimetry (ITC)

Precipitates were removed from protein and ligand samples by centrifugation at max speed (>10000xg) in an Eppendorf 5414C microcentrifuge (Eppendorf) at 277K for 5min. Samples were then degassed and thermoequilibrated in a ThermoVac device (MicroCal; Northampton, MA, USA). Approximately 1.3mL of 25.5μM RNBec_N22 was loaded into the sample cell of a VP-ITC MicroCalorimeter (MicroCal) and thermoequilibrated at 303K. From the excess sample loaded into the sample cell, a small sample (50μL) was removed and quantified by denaturing absorbance spectroscopy at 280nm. Approximately 350μL of 106μM dA(30) (ligand) was loaded into the injection syringe. After two purge-refill cycles of the injection syringe, a small sample of dA(30) (10μL) was removed and quantified by measuring absorbance at 260nm. The injection syringe was inserted into the sample cell and a reference power baseline was established at 0.055J/s during which the injection syringe was in stirring mode at 450RPM. Once the reference power baseline was established, the experiment began. Following the baseline data collection, 10μL of dA(30) was titrated into the sample cell over a period of 20s followed by 240s during which no sample was injected. A total of 30 injections were performed for the experiment. The resulting data was analyzed in Origin software (MicroCal). Peaks corresponding to the power required to keep the sample cell at the same temperature as the reference cell during each injection were integrated and plotted as a function of DNA concentration. Binding constants were obtained by curve fitting the data (See Appendix A) (Fersht, 1999).

2.7 Measurement of Binding by Electrophoretic Mobility Gel Shift Assay (EMSA)

40μM of RNBec_N22 was incubated with 400μM of dA(30) in 20μL RNB buffer for approximately 10min before loading onto a Native PAG to separate bound RNase II/DNA complexes from free RNase II. Protein was detected with the silver staining method as described in 3.3.1.4.

Chapter 3: Experimental Results

3.1 Domain Mapping by Studying the Effect of Domains on Processivity and Exoribonucleolytic Activity

3.1.1 Background – C-terminal Deletion Mutants

Work in the Mosimann lab with RNase II deletion mutants lacking small portions of the C-terminus (c10 and c25, illustrated in figure 7) shows an accumulation of degradation intermediates not present in assays with full-length RNase II (data not shown). These degradation intermediates suggest that the RNase II mutants remove a specific number of nucleotides – fewer than the full-length protein removes – prior to dissociation from the *rnb* transcript. Following dissociation, the deletion mutants bind a new *rnb* transcript and begin degradation. Full-length RNase II degrades the chain to completion, leaving as products a small oligoribonucleotide and mononucleotides, with no degradation intermediates. This full-length RNase II activity shows up on a gel simply as a disappearance of full-length RNA. The small C-terminal deletions may be disrupting the processive activity of RNase II by causing misfolding of the bioinformatically predicted C-terminal S1 oligonucleotide/oligosaccharide binding (OB) domain. Following the publication of the crystal structure of RNase II, this S1 domain was found to be a part of the putative anchor region of RNase II that binds RNA, proposed by Cannistraro and Kennell (1999).

The secondary structure of the *rnb* transcript was analyzed with GENEBEE RNA secondary structure prediction software (Brodsky et al., 1995; Brodsky et al., 1992). The stability of secondary structure elements suggest that full-length RNase II should have little trouble degrading the entire *rnb* transcript. The maximum melting temperature of

secondary structure predicted by GENEBEE in the *rnb* transcript is 313.4K according to Integrated DNA Technology's (IDT) Oligoanalyzer tool. This is the single melting temperature that exceeds the reaction conditions of 310K, and therefore it is likely to be the single region of secondary structure at this temperature. The accumulation of degradation products may be a result of the inability of the C-terminal deletion mutants to degrade through the secondary structure through which full-length RNase II is known to degrade. However, this secondary structure is predicted to include nucleotides 1718-1725, approximately 200 nucleotides from the 3' end; the size of the degradation intermediate is not in this range.

In order to generate a domain map of RNase II, a series of C-terminal deletion mutants was constructed (Figure 7), and their activity analyzed. The C-terminal deletions were generated using as guides either known or predicted inter-domain linkers. An alignment of the RNase II primary sequence to primary sequences with known structural domains predicts homology between a region of the C-terminus and an S1 OB domain. The c60 deletion mutant was based on the removal of this S1 domain. The remaining three deletion mutants were constructed by analyzing the primary protein sequence with the Scooby Domain inter-domain linker prediction Java applet using the Eisenberg option (George et al., 2005; Pang et al., 2008). With the publication of the structure of RNase II (Frazao et al., 2006; Zuo et al., 2006), the C-terminal deletion mutants can be evaluated for their accuracy in the prediction of interdomain linkers. The crystal structure of the protein confirms the presence of the three bioinformatically predicted OB domains. These domains include two cold-shock domains (CSD) at the N-terminus and an S1

domain at the C-terminus (See figure 3 and 4 in introduction). The remainder of the protein is a

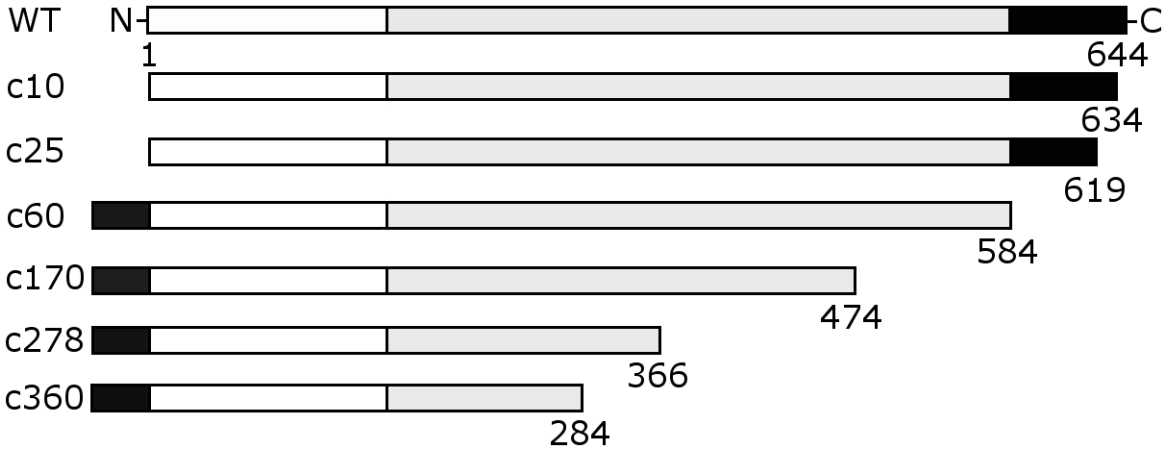

Figure 7. Linear Representation of the C-terminal Deletion Mutants: Numbers at the C-terminus indicate the terminal amino acid. The black boxes at the N-terminus of c60, c170, c278 and c360 represent a 22-residue Histidine affinity tag. The grey shaded area in all constructs represent the region of the sequence termed RNB by Frazao et al (2006) that is unique to RNase II-like proteins. Black boxes at the C-terminus of WT, c10 and c25 indicate an S1 oligonucleotide/oligosaccharide binding (OB) domain.

sequence unique to RNase II-like proteins. The domains present in this region (as shown by the crystal structure) are composed of non-contiguous sequences. Inter-domain linker prediction programs only identify domains composed of contiguous sequences. As a result, the removal of entire domains using the Scooby Domain inter-domain linker prediction program was inaccurate. The c60 mutant is the most soluble of the deletion mutants, however, it is not as hardy as the wild-type, requiring modified overexpression conditions using a reduced temperature of 303K. These milder overexpression conditions result in far smaller quantity of overexpressed protein from a 1L preparation than can be obtained with wild-type protein. The c60 mutant has a truncation that is closest to the removal of a full domain with nearly the entire S1 domain removed. According to the crystal structure, however, there are still approximately 25 residues of the S1 domain left.

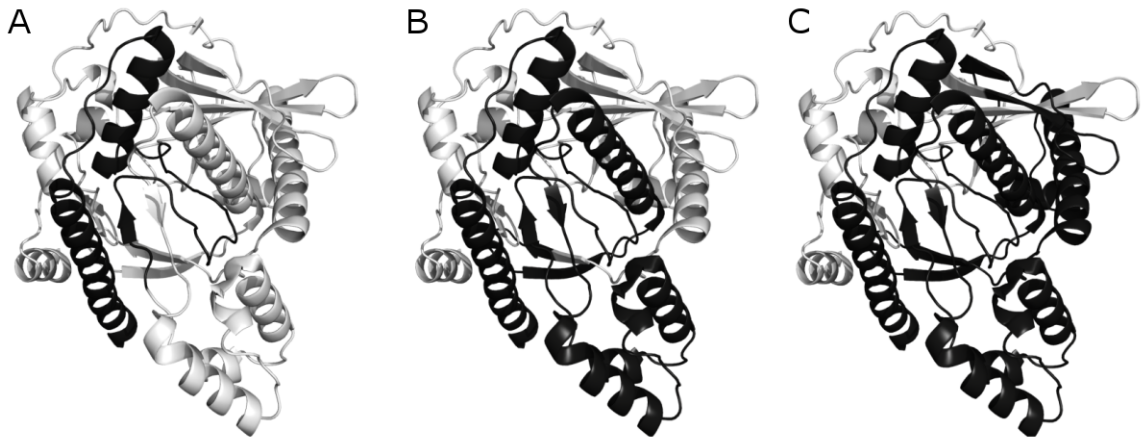

Figure 8. Residues Removed from RNB Domain in C-terminal Deletion Mutants: RNB domain showing the structure that has been removed as a result of C-terminal deletion mutants. In each panel, the black structure is absent in that panel's respective mutant; A- c170; B- c278; C- c360

It is likely that the removal of the majority of the S1 domain effectively eliminates any function of the S1 domain related to its structure. The c170 mutant is only sparingly soluble; overexpression conditions are similar to c60, but not as much protein is produced. The c170 mutant removes an α-helical inter-domain linker and approximately twenty-five additional residues that are a component of the complex multi-domain structure termed the RNB domain (Figure 8) (Amblar et al., 2006). The absence of these twenty-five residues likely causes some misfolding, but not complete denaturation, of the RNB domain. In addition, there is an independent folding unit within the RNB domain between residues 418 and 472 that is not affected by the truncation. Both the c278 and c360 mutants terminate in the middle of a β-sheet and are insoluble. In the c278 mutant, the folding unit between residues 418 and 472, as well as nearly one third of the residues of the RNB domain, is absent (Figure 8B). In the c360 mutant an additional third of the residues from the RNB domain are removed (Figure 8C). It is likely that these deletion mutants cause significant denaturation of the RNB domain.

3.1.2 RNase Assay

In order to assess the activity of the C-terminal deletion mutants, a novel degradation assay was developed. The results of the non-radioactive assay are visualized by staining with ethidium bromide after electrophoretic separation. The RNA genome of the bacteriophage MS2 is used as a substrate. MS2 RNA is easy to visualize by staining with ethidium bromide (see figures 9A and 9B) due to its large size – 3569 nucleotides (Fiers et al., 1976). The size and nearly random nucleotide distribution of MS2 RNA provides the potential for the formation of secondary structure. Using IDT's OligoAnalyzer tool, MS2 is predicted to have only two secondary structures that are stable above 310K. Secondary structure is an inevitability, and a substrate with secondary structure more accurately represents a substrate that RNase II must degrade *in vivo*. An increase in sensitivity to secondary structure by RNase II C-terminal deletion mutants would be detectable when using MS2 RNA. Additionally, the length of MS2 RNA provides an opportunity to study the number of nucleotides over which RNase II remains processive. Homoribopolymeric RNAs of less than one hundred nucleotides are not suitable for the purpose of studying the effect of secondary structure. In addition, it does not provide nearly the same length as MS2 RNA does to study how long RNase II maintains processivity. In these ways, MS2 RNA is better suited as a substrate that would provide results that more accurately reflect the *in vivo* function of RNase II.

Finally, the assay can provide crude kinetic data relating the disappearance of full-length RNA to protein concentration, providing association rate constants and turnover numbers.

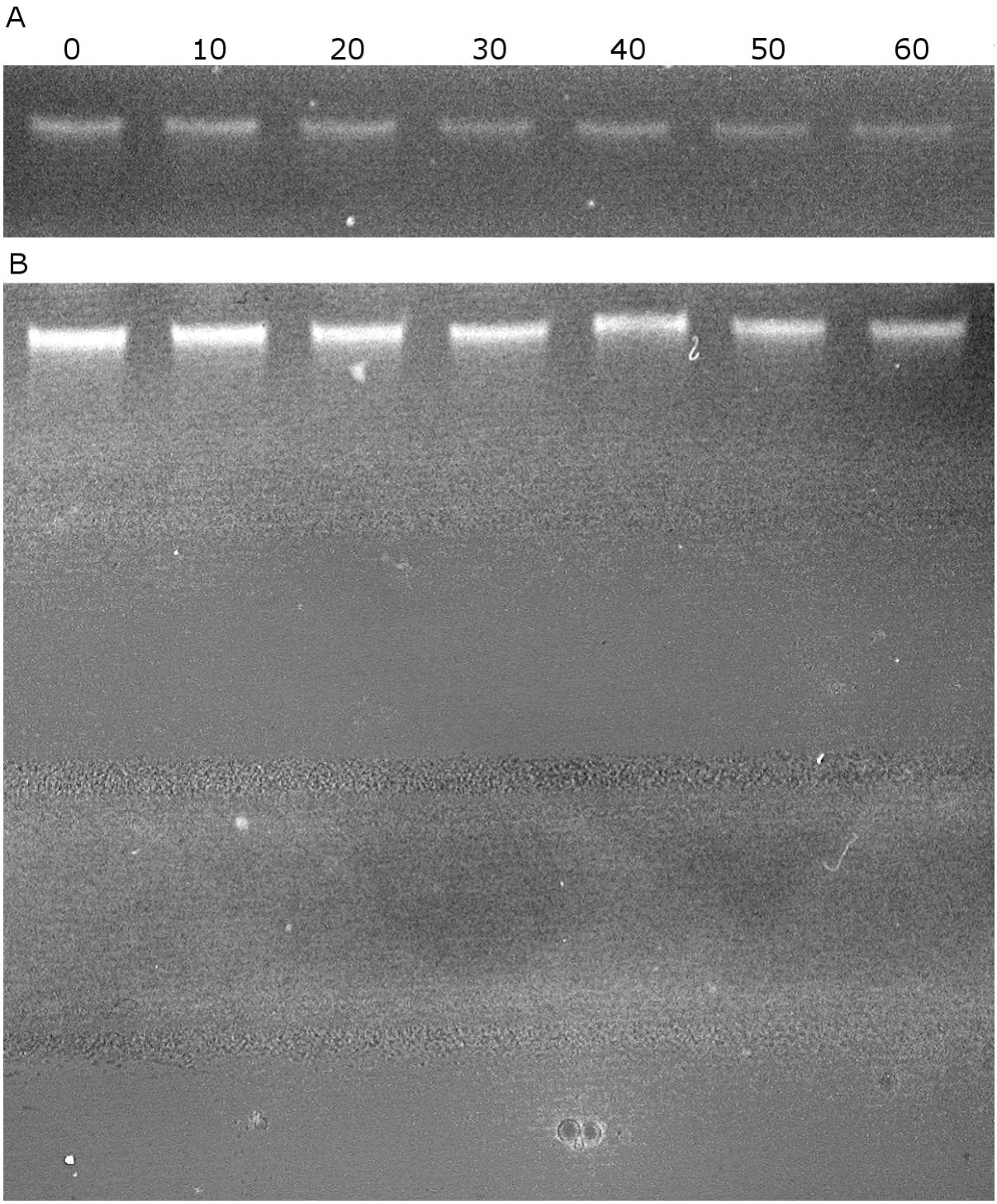

Figure 9. RNase Assay of RNBec_N22 and RNBst_N22: Numbers indicate the time in minutes the MS2 RNA sample was incubated at 310K. A: 1µM RNBec_N22; B: 1µM RNBst_N22. Note the absence of bands at higher mobility in Panel B.

Although the action of RNase II on other physiological substrates has been studied (Amblar and Arraiano, 2005a, b; Coburn and Mackie, 1996a; Kaplan and Apirion, 1974;

Marujo et al., 2000; Mohanty and Kushner, 2000, 2003), it has largely been for the identification of RNase II specific substrates; little to no kinetic data has been generated using physiological substrates.

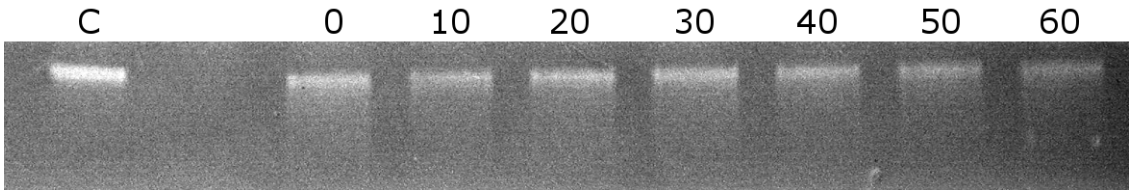

Figure 10. RNase Assay of RNBec_c60: Typical degradation profile of MS2 RNA by 10μM RNBec_c60. Numbers indicate the time in minutes the sample was incubated at 310K. C indicates unincubated RNA.

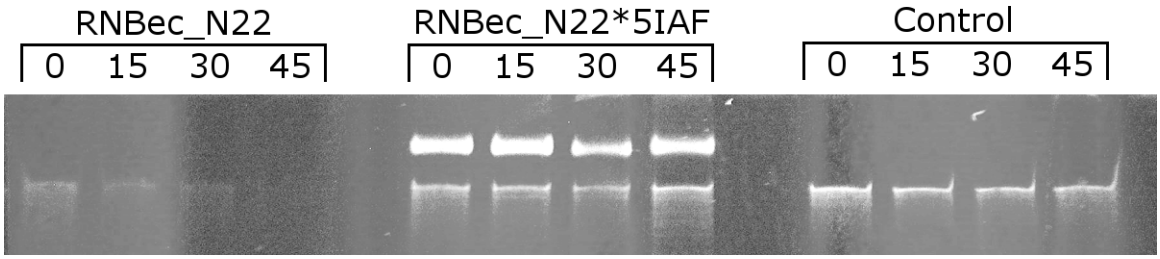

Figure 11. RNase Assay of RNBec_N22*5IAF: Comparison of MS2 RNA degradation by RNBec_N22 (10μM) and RNBec_N22*5IAF (10μM). Numbers indicate the time in minutes the sample was incubated at 310K. Control reactions were incubated without any enzyme. In lanes with doublets, the top band is RNBec_N22*5IAF and the bottom is MS2 RNA.

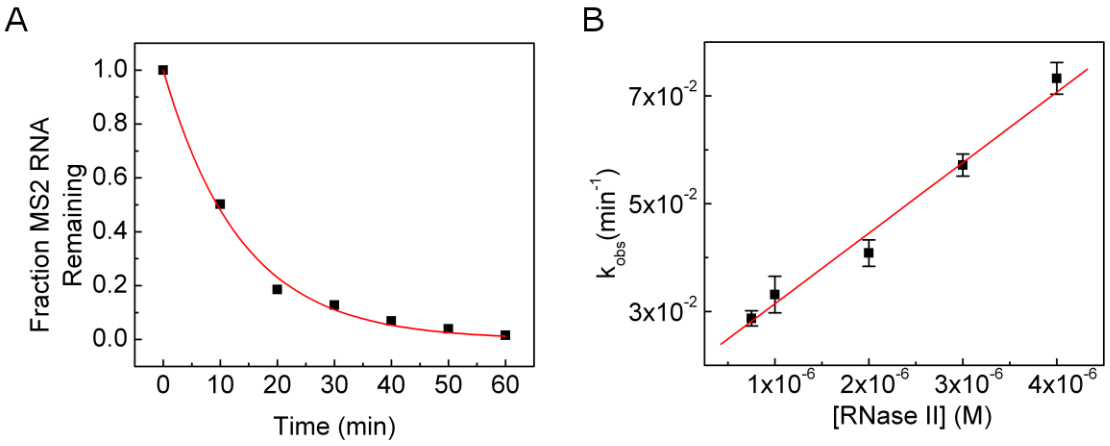

Figure 12. Kinetics of Association Between RNBec_N22 and MS2 RNA. A- Association curve obtained by measuring the fraction of MS2 RNA remaining in degradation assay with 4μM RNBec_N22. B- Plot of apparent rate constants as a function of RNBec_N22 concentration**.**

Degradation of MS2 RNA by 1μM RNBec_N22 (Figure 9A) was studied on a qualitative scale, and compared to 1μM RNBst_N22 (Figure 9B), 10μM RNBec_c60 (Figure 10) and later, 10μM RNBec_N22*5IAF (Figure 11). RNBec_c60 and RNBec_N22*5IAF were studied at higher concentrations because there was no apparent degradation of MS2 RNA when using 1μM protein. As figures 10 and 11 illustrate, even at elevated concentrations these two variants are impaired in their ability to degrade MS2 RNA. RNBec_N22 is slightly better at degrading MS2 RNA than RNBst_N22. A striking feature of this assay is the absence of any intermediate band sizes (see figure 9B). If there is any dissociation of RNase II from the MS2 RNA at sites of secondary structure, there would be an accumulation of a smaller band as the larger band loses intensity. Although there is no accumulation of a smaller band, assays using RNBec_c60 show some smearing below the main MS2 RNA. This suggests that the deletion of the C-terminal 60 residues causes RNase II to become distributive. The appearance of distributive activity could be a result of a decrease in affinity. This agrees with the study by Amblar *et al* (2006), in which the deletion of the S1 domain causes a decrease in affinity between RNase II and a 30 nucleotide RNA oligomer. The degradation of MS2 RNA by RNBec_N22 was studied on a quantitative scale over 60min, using 0.75μM to 4.0μM protein. To analyze kinetic properties, results were densitometrically quantified in IMAGEJ software (Abramoff et al., 2004). A hyperbolic curve (Goodrich and Kugel, 2007) was fit through the resulting plot to obtain an apparent rate constant (see Appendix A).

A typical degradation curve is seen in figure 12A. A plot of the observed association constant as a function of RNase II degradation (Figure 12B) yields an association

constant of $0.02M^{-1}min^{-1}$. In addition, analysis of the initial rates of the degradation curve in figure 12A gives a turnover rate of approximately 6nt/s. To date there have been no published association rate constants, but the published turnover rate of RNase II on polyadenylate RNA (the preferred substrate) is 70nt/s (Cannistraro and Kennell, 1994), approximately 10-fold higher than determined here.

3.2 Progress Towards a Fluorescent Binding Assay

One of the goals of this project is to use fluorescence to observe the structural dynamics of RNase II during hydrolysis. A prerequisite for these studies is the development of a fluorescence-based binding assay. This fluorescent binding assay will not only confirm and quantify binding interactions of mutant RNase II proteins, it will also provide a starting point for measuring the kinetics of hydrolysis, provided the fluorescence changes during a hydrolysis or translocation event. In these binding studies, DNA – a known competitive inhibitor and non-hydrolysable analogue (Cannistraro and Kennell, 1994, 1999; Gorelic and Apirion, 1971; Spahr, 1964) – was used in place of RNA in order to simplify the system by eliminating the steps of RNA hydrolysis and translocation, which would complicate signal interpretation.

Experiments were designed in an attempt to identify binding events by following the changing fluorescent intensity of fluorophores on RNase II as a function of increasing substrate concentration. It is known that a change in the quantum yield of a fluorophore – a value relating the number of emitted photons to the number of absorbed photons (see Appendix A) – results in a change in fluorescent intensity. In addition, quantum yield can be affected by a change in the local electronic environment of a fluorophore (Lakowicz, 1999). This sensitivity to changes in the local environment of a fluorophore can be

exploited to follow binding interactions. These changes may be located either at the site of binding or a site distal from the binding site, induced by conformational changes in connecting structure.

3.2.1 Measurement of Natural Protein Fluorescence

With 9 tryptophan residues (a naturally fluorescent amino acid) in the 644 amino acid RNase II, the probability of at least one tryptophan residue experiencing a change in its local environment upon binding of DNA is reasonably good. In order to test this hypothesis, dA(30) was titrated into a solution containing RNBec_N22, and the intrinsic protein fluorescence was measured as a function of dA(30) concentration. The fluorescent intensities at wavelengths 5nm below to 5nm above the emission maximum of tryptophan (340nm) were averaged and plotted as a function of dA(30) concentration, and generates a binding curve yielding a dissociation constant of approximately 30μM (Figure 13) (see Appendix A). This value is three orders of magnitude higher than the published binding constant obtained with a 30nt RNA oligomer as a ligand (Amblar et al., 2006; Frazao et al., 2006).

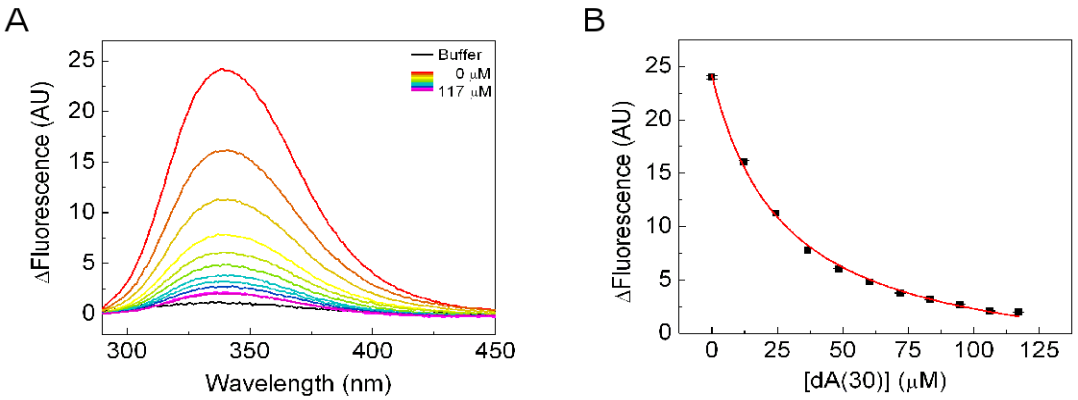

Figure 13. Measurement of Binding by Direct Excitation of Tryptophan: Binding of dA(30) oligomer to RNBec_N22 observed by illuminating sample at 280nm and measuring fluorescence at 290-450nm. A - Spectra of RNBec_N22 when titrated with dA(30) oligomer; B Titration curve of dA(30) DNA oligomer into RNec_N22.

3.2.2 Measurement of Non-Natural Protein Fluorescence

In order to confirm the dissociation constant measured above, an alternative method to measure binding was tested by following the change in fluorescence of a non-natural, protein-associated fluorophore as a function of substrate concentration.

A common method of fluorescently labeling proteins is to covalently modify the thiol group of a cysteine residue with thiol-reactive fluorescent dyes. The targeting of cysteine residues allows for more selective labeling, as cysteine residues appear relatively rarely in proteins. In extreme cases where a protein has a single cysteine residue, this can be advantageous. Labeling of a single cysteine in the presence of a second fluorophore allows for FRET interactions to take place, allowing a study of dynamic interactions. However, as the number of cysteines, and thus the number of fluorescent dyes, increases so too does the complexity of the signal that must be interpreted. In addition, cysteine

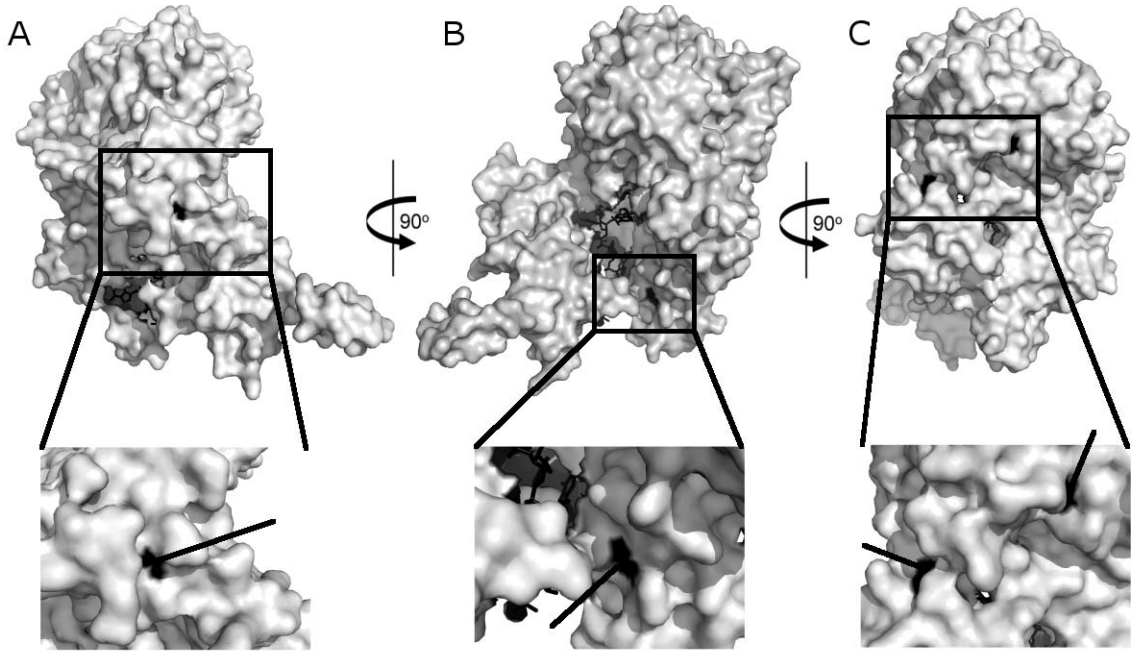

Figure 14. Molecular Surface of RNase II: Cysteine residues accessible to the solvent are identified in black. A - Identifies cysteine 112; B; Identifies cysteine 603; C - Identifies cysteines 344 and 450.

residues tend to be functional, and modification of a functional thiol group negatively impacts activity. As these functional cysteines tend to be conserved among homologues, an analysis of conservation may be directive in identifying functional cysteines. Three of the cysteines (271, 284, 399) in RNase II appear in at least 50% of the 115 bacterial RNase II homologues, with one (271) present in 70% of homologues. The remaining four cysteines (112, 344, 450, and 603) appear in fewer than 40% of the homologues, suggesting that the functional importance of these cysteines is limited. Prior to the publication of the RNase II crystal structure, no information was available about the location of the cysteines, making it difficult to determine the location of functional cysteines. However, following the publication of the RNase II crystal structure, it was possible to identify cysteines that are likely to be accessible to the solvent, and therefore susceptible to targeting with fluorescent dyes. Analysis of the RNase II surface residues shows that the four cysteines with the least conservation appear on the surface of RNase II (Figure 14), making them good targets for fluorescent labeling. RNase II was labeled with 5-IAF, a thiol-reactive fluorescein derivative that is very sensitive to changes in its local environment. Typically, 63% of the RNase II subjected to the labeling reaction was recovered. This sample was spectroscopically quantified under denaturing conditions at 280nm and 492nm (the latter value is the absorbance λ_{max} of 5-IAF), and was found to be labeled in a 0.6:1 ratio of dye to protein. This ratio suggests that there is a large portion of the RNase II population that is not fluorescently labeled. Of the labeled RNase II molecules, it cannot be determined with the techniques used here the population of RNase II molecules bearing a single 5-IAF molecule. This is due to the presence of more than one solvent accessible cysteine and the resulting possibility that

some RNase II molecules may bear more than one 5-IAF molecule. A plot of the fluorescence at the emission maximum of 5-IAF (525nm; data points are the average fluorescence of 520-530nm) revealed no change in fluorescence as a function of increasing dA(30) concentration (Figure 15). Lack of change in the fluorescent signal may be reporting one of three results. First, there may be no binding events taking place under these conditions. It is unlikely that no binding is occurring, as DNA oligomer has been reported to have a K_i of approximately 30μM (Cannistraro and Kennell, 1994). Second, it is possible that the fluorescence of bound 5-IAF simply does not reflect binding events. Figure 14 shows that there are three cysteine residues that are located on parts of RNase II that are nowhere near the binding site. It is possible that binding does not alter the local environment of residues 112, 344 or 450. Third, it is possible that labeling interferes with binding. For example, cysteine 603 is located in the S1 domain, which is known to be important for binding (Frazao et al., 2006). As a result, labeling of cysteine 603 may prevent binding of nucleic acid to RNase II. Clearly, another fluorescent binding assay is required to confirm the initial binding results.

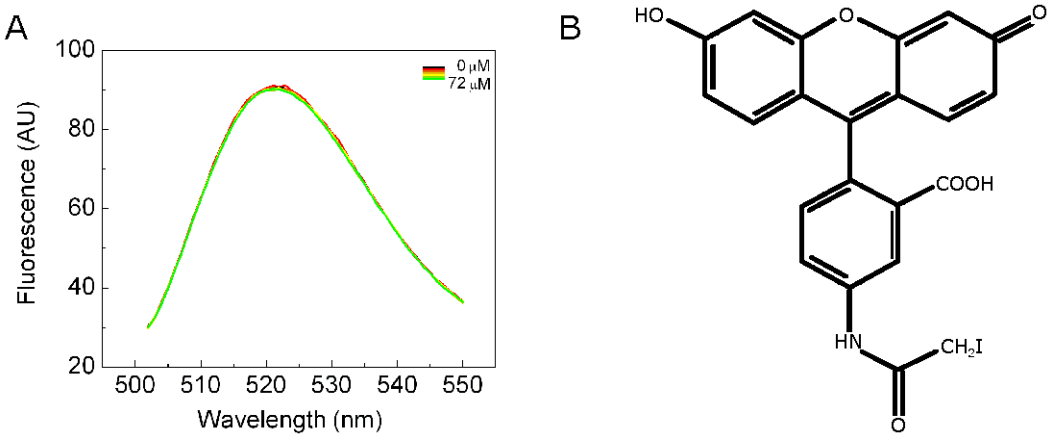

Figure 15. Measurement of Binding by Direct Excitation of 5-IAF: A- Spectra of RNBec_N22*5IAF when titrated with dA(30) oligomer and excited at 492nm. B- Structure of 5-IAF.

3.2.3 Measurement of Fluorescence Resonance Energy Transfer (FRET)

FRET occurs when a pair of fluorophores come into molecular proximity and transfer energy through a resonance mechanism. In FRET, a pair of fluorescent dyes is selected based on the spectroscopic properties of each dye. The dyes are chosen so that the emission spectrum of one fluorophore – called the donor – overlaps with the absorbance spectrum of the second dye – called the acceptor. This is described by the overlap integral. In this type of system, the donor fluorophore can be excited, and when in molecular proximity to the acceptor fluorophore, transfers energy to the acceptor in a radiationless process, causing acceptor dye fluorescence. The extent to which energy is transferred can be quantified by a value known as the FRET efficiency, which is described in Appendix A. A unique property of a particular dye pair that is intrinsically related to the FRET efficiency is a value called the Förster distance. The Förster distance is the distance at which the transfer of energy between the two fluorophores is 50%. When the distance between the fluorophores reaches a critical distance of approximately twice the Förster distance, the transfer efficiency reaches 1.56% (Lakowicz, 1999). If the dyes are any further apart than twice the Förster distance they effectively cease their transfer of resonance energy. The interaction between the two fluorophores over a range of twice their Förster distance is very sensitive; the FRET efficiency can be directly related to the distance separating the fluorophores (Lakowicz, 1999).

In the case of RNase II, the two fluorophores are intrinsic tryptophans and a 5-IAF molecule. A change in FRET efficiency as a function of increasing ligand concentration will report conformational changes associated with ligand binding. The overlap integral of L-tryptophan and 5-IAF was evaluated in order to determine the suitability of

tryptophan and 5-IAF as a FRET dye pair (Figure 16A). The small overlap integral indicates that FRET may occur. Although an experiment with these fluorophores would not be designed for the sole purpose of FRET, their presence on RNase II provides an opportunity to observe a relative movement between 5-IAF and one or several tryptophan residues, reflecting the conformational changes that may occur during binding.

The availability of the RNase II crystal structure during these experiments allowed the measurements of distances between RNase II's intrinsic tryptophan residues and cysteine. This analysis revealed numerous distances less than 40Å (Table 7), a distance over which this pair of fluorophores has been shown to interact (Zukin et al., 1977). The presence of fluorescence at the emission maximum of 5-IAF (525nm) when RNBec_N22*5IAF was excited at 280nm indicated that there is a resonance energy transfer between tryptophan and 5-IAF. The addition of dA(30) caused a change in fluorescence intensity of both tryptophan and 5-IAF (Figure 16).Titration curves were obtained by plotting the average fluorescence across 10nm centered on the emission maximum of both tryptophan (340nm) and 5-IAF (525nm) as a function of increasing dA(30) concentration. Curve-fitting of the data (see Appendix A) results in nearly identical K_d values of 32μM when measured by tryptophan emission and 29μM when measured by fluorescein emission (Figure 16C). These values match very well with the dissociation constant obtained by measuring tryptophan fluorescence (30μM). However, both Plots show a decrease in fluorescence. This type of correlation between fluorophores is not consistent with a typical change in FRET efficiency as a result of a change in distance between two fluorophores. Rather than a reciprocal relation between donor and acceptor fluorescence typically seen when the distances between the

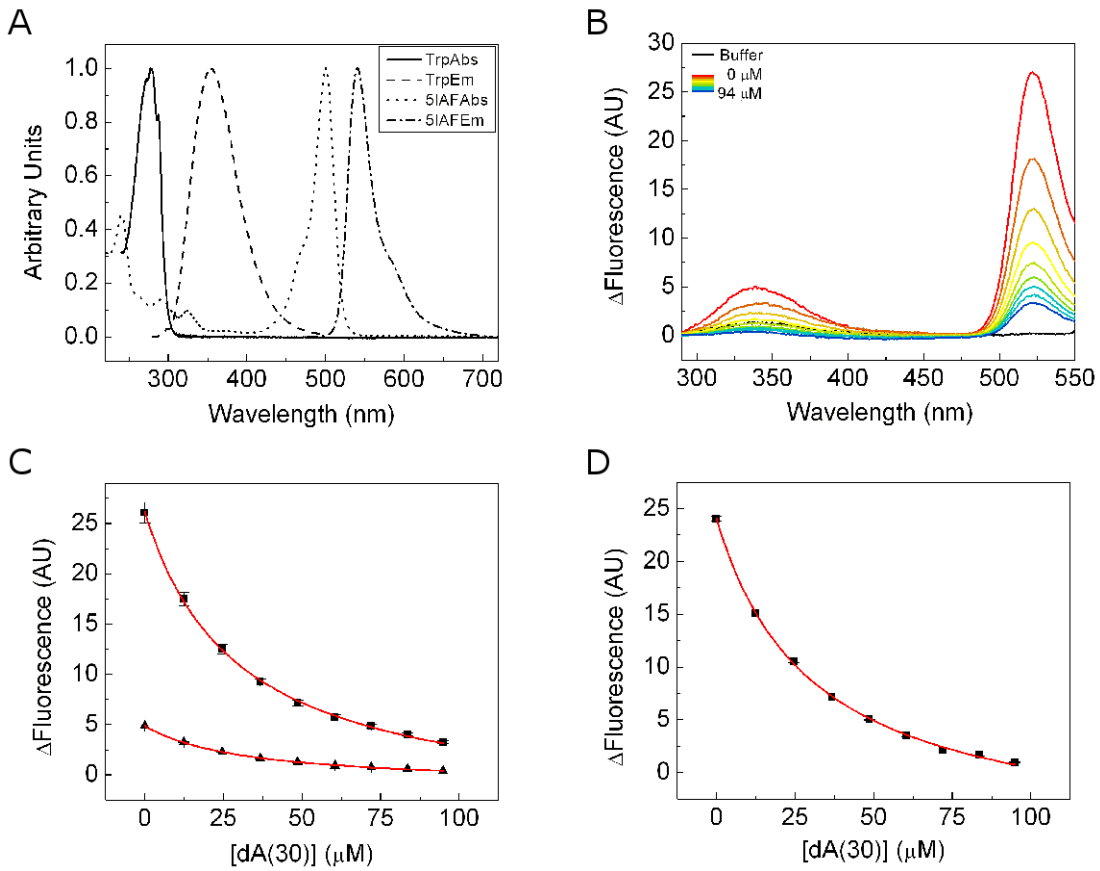

Figure 16. Measurement of Binding by FRET Between Tryptophan and 5-IAF: Binding of dA(30) DNA oligomer to RNBec_N22*5IAF observed by illuminating sample at 280nm and reading fluorescence at 290-550nm. A - Absorbance and Emission spectra of L-tryptophan and 5-iodoacetamidofluorescein; B - Spectra of RNBec_N22*5IAF when titrated with dA(30) oligomer; C - Titration curves of dA(30) DNA oligomer into RNBec_N22*5IAF measured using 5IAF fluorescence (top curve) and tryptophan fluorescence (bottom curve); D - Titration curve of dA(30) DNA oligomer into L-tryptophan.

Table 7: Distances (in angstroms) separating the S_γ of cystidyl residues from the C_δ of tryptophyl residues in RNase II. Distances in grey cells are distances under 40 angstroms.

	Trp127	Trp161	Trp162	Trp234	Trp319	Trp326	Trp350	Trp495	Trp548
Cys112	13	25	21	48	62	58	59	50	21
Cys344	45	32	40	33	14	19	14	17	38
Cys450	47	37	44	41	33	38	12	21	39
Cys603	34	34	40	60	53	54	45	29	47

fluorophores change, there is a direct relation between donor and acceptor fluorescence. This is most likely reporting that the fluorescein is receiving less energy from tryptophan not because fluorescein is further away, but because tryptophan fluorescence is being quenched by another process. Studies on the interaction of tryptophan mono- and

tripeptides show that tryptophan fluorescence can be quenched by the adenine bases of oligomeric adenylate (Toulme et al., 1974). To test the hypothesis that tryptophan is quenched by adenine bases in these experiments, free L-tryptophan was titrated with dA(30) under the same conditions as in the FRET experiment. Analysis of the data with an equation used to obtain binding constants gives a value of 29μM (Figure 16D). This change in fluorescent signal obtained in from these experiments is a result of a quenching event. That the values of the previous fluorescence binding experiments are the same suggest that these data are also reporting quenching.

3.2.4 Measurement of Non-Natural Ligand Fluorescence

Experiments using fluorescently labeled protein did not generate any dissociation constants. An alternative to using a fluorescently labeled protein as a reporter of binding events is to use a fluorescently labeled ligand.

2-aminopurine (2-AP) is a fluorophore that is structurally similar to adenine (Ward et al., 1969) and has previously been used in studies of nucleic acid conformation (Malta et al., 2006). A particularly useful property of 2-AP relates to its fluorescence in different local environments; 2-AP is less fluorescent when it is base-stacking with another aromatic compound, such as an adenine base, than when it is not base-stacking. This property has been exploited in a study of nucleotide excision repair proteins (Malta et al., 2006) to identify bases that have been flipped out of a DNA duplex. In addition, 2-AP is almost two orders of magnitude more fluorescent when in free nucleotide form than when it is a part of a nucleotide chain (Ward et al., 1969), a useful property that may be exploited to monitor cleavage events. Based on the currently available crystal structure of RNase II in complex with RNA, we designed a binding assay that would exploit the effect of

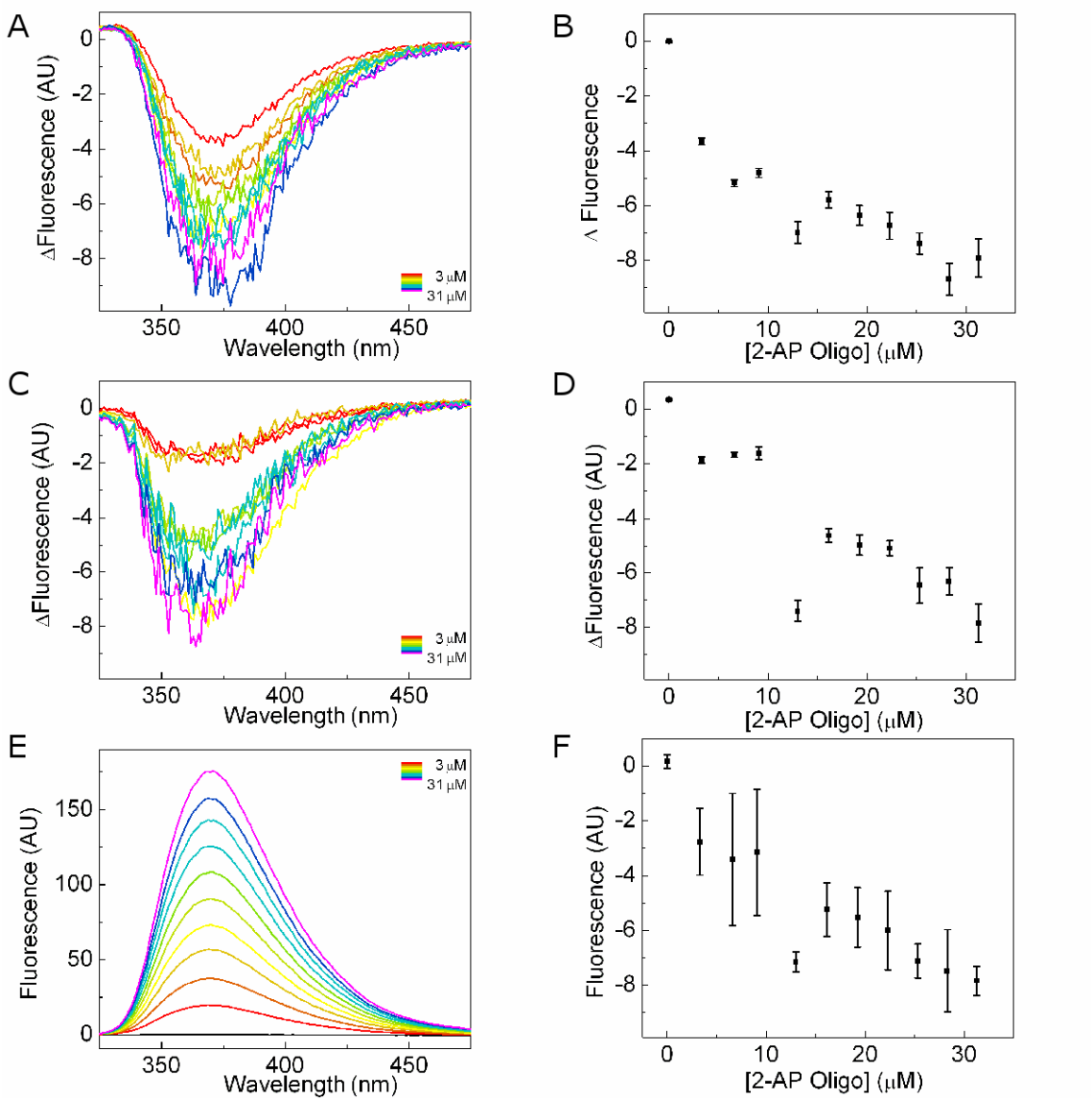

Figure 17. Measurement of Binding by Direct Excitation of 2-AP: Binding of dA(30)-2-AP to RNBec_N22 observed by illuminating sample at 310nm and measuring fluorescence at 325-475nm. A, C - Difference spectra of RNBec_N22 when titrated with dA(30)-2-AP for three individual experiments; B, D - Titration curve of dA(30)-2-AP into RNBec_N22 for A and C respectively; E - Typical experimental fluorescence spectra; F - Titration curve combining data from B and D.

conformation on fluorescence. The RNase II structure shows 5 nucleotides at the 3' end of the RNA chain clamped into a base-stacked arrangement by a phenylalanine side-chain at the 5' end and a tyrosine side-chain at the 3' end. The sixth nucleotide from the extreme 3' end however, is not participating in any base-stacking interactions (Figure 6). With the assumption that a 30 nucleotide, single-stranded DNA molecule in an aqueous

environment adopts a helical conformation where all bases are stacked, a substrate – hereafter referred to as dA(30)-2-AP – was designed with a 2-AP residue at the sixth position from the 3' end. This would take advantage of the change in the fluorescence of 2-AP when it shifts from base-stacked conformation (unbound) to non-base-stacked conformation (bound). With wild-type RNase II in the sample cuvette, dA(30)-2-AP was titrated into the RNase II solution. Only a small fluorescent change was observed (Figure 17; compare panel E with panels A and C), and the signal to noise ratio is not favorable for determining binding. In an attempt to reduce the signal to noise ratio of the binding assay, the system was reversed so the titrant does not add significant fluorescence to the system. In order to do this, the dA(30)-2-AP was in the cuvette, and was titrated with the RNase II, which does not fluoresce at the excitation wavelength used (310nm). A plot of the data revealed a nearly linear plot of fluorescence as a function of increasing protein concentration with what appears to be the beginning of a saturation point at higher protein concentrations. The K_d of this curve is 180µM with a standard deviation of 40µM

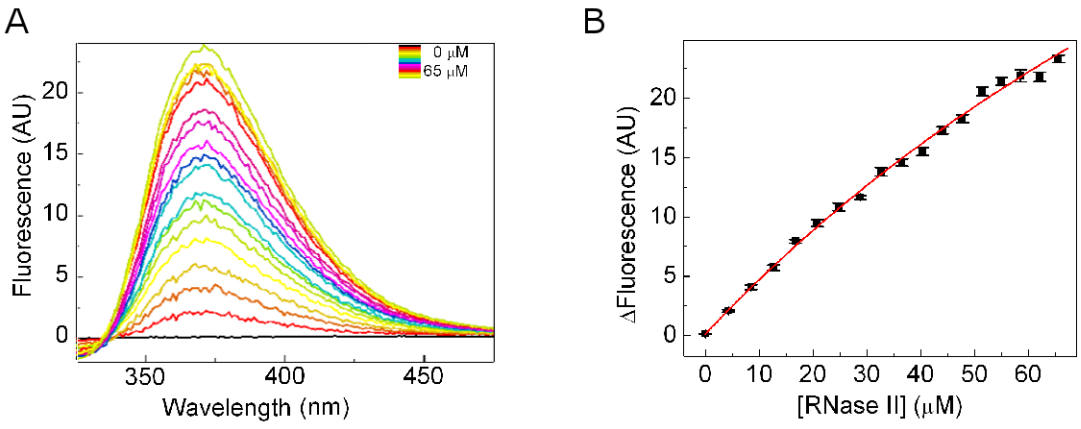

Figure 18. Measurement of Binding by Direct Excitation of 2-AP: Reversal of Experimental Set-Up: Binding of dA(30)-2AP to RNBec_N22 observed by illuminating sample at 310nm and measuring fluorescence at 325-475nm. A - Spectra of dA(30)-2AP when titrated with RNBec_N22; B - Titration curve of RNBec_N22 into dA(30)-2AP.

(Figure 18B).This titration was performed to a maximum protein concentration of 70µM. Beyond this concentration, no information can be gathered, as the C-terminal deletion mutants cannot be purified to this concentration.

3.2.5 Protection of Ligand Fluorescence from Quenching

As seen in figure 18 above, there is an indication of saturation at higher concentrations. However, the binding constant obtained from this curve is inaccurate as indicated by the large standard deviation. In order to amplify the change in fluorescence upon binding, an assay was designed to exploit the quenching of 2-AP by acrylamide. In this quenching assay, the fluorescence of unbound dA(30)-2-AP would be reduced by acrylamide, a quenching agent. Binding of RNase II to dA(30)-2-AP would protect 2-AP from the acrylamide, thus increasing the fluorescence of the system. Based on the study by Malta *et al* (2006), RNase II was titrated into 1.5µM dA(30)-2-AP in the presence of 300mM acrylamide. As seen in the experiments where RNase II was titrated into dA(30) in the absence of a quenching agent, a linear plot was observed (Figure 19). Unfortunately, the

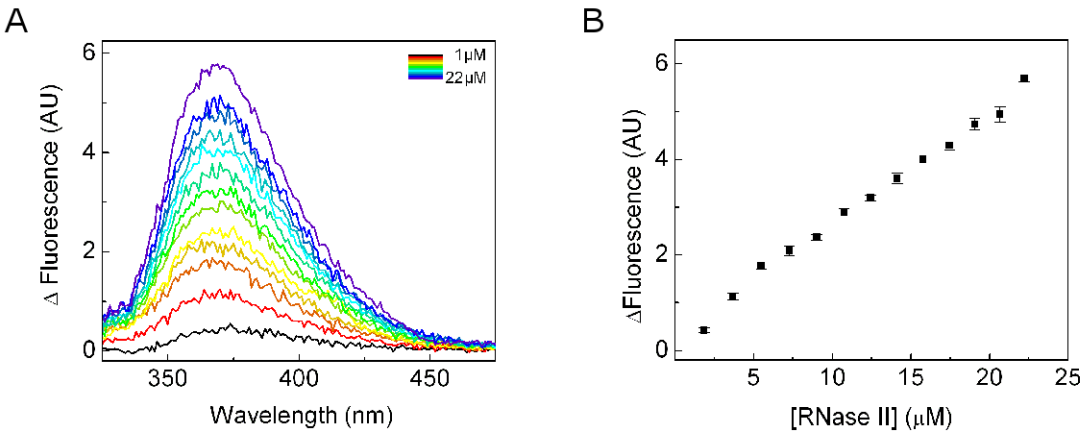

Figure 19. Measurement of Binding by Protection of 2-AP from a Quenching Agent: Binding of dA(30)-2AP to RNBec_N22 in the presence of 300mM acrylamide, observed by illuminating sample at 310nm and reading fluorescence at 325-450nm. (a) - Spectra of dA(30)-2AP when titrated with RNBec_N22, corrected for presence of dA(30)-2AP and protein; (b) Titration curve of RNBec_N22 into dA(30)-2AP in the presence of 300mM acrylamide.

increase in fluorescence intensity upon addition of RNase II is no greater than in the same experiment without a quenching agent. A binding constant was not determined because the curve did not show any indication of saturation, which is required for the determination of a binding constant. This experiment was intended to increase the values of the difference spectra; its inability to do so makes it no more useful than those in section 3.2.4.

3.3 Measurement of Binding by Isothermal Titration Calorimetry

Concurrent with the fluorescence studies, non-radioactive, non-fluorescent ITC experiments were conducted to provide an additional verification of any binding results generated with the fluorescent assays. In addition to its usefulness in confirming binding results, it is also useful in providing thermodynamic data regarding binding events. To date, there have been no thermodynamic investigations into the binding between RNase II and nucleic acids. Under conditions where a binding event generates a strong thermal signal, isothermal titration calorimetry is a very effective and sensitive method for studying not only binding events, but also the thermodynamic properties of binding events. Using a series of experiments conducted at different temperatures, a heat capacity can be generated. From these experimentally determined heat capacities and binding constants, enthalpic and entropic values can be inferred.

The main adiabatic chamber of an ITC instrument contains a sample cell and reference cell. The sample cell contains the experimental sample while the reference cell contains a solution identical to that in the sample cell minus the macromolecule being studied. The cells are connected to an extremely sensitive heat monitoring system and a power cell. The instrument responds to a loss or gain of heat in the sample cell by adjusting the

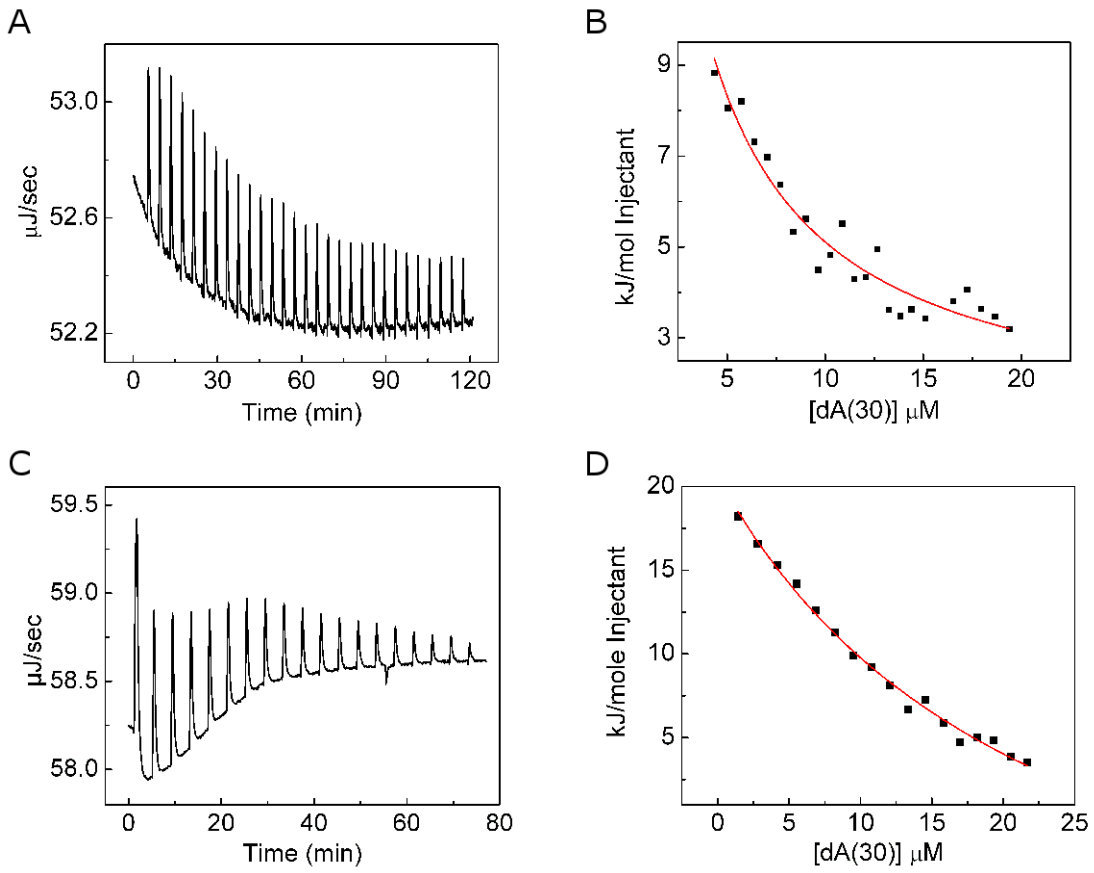

Figure 20. Measurement of Binding by ITC: ITC binding assays using RNBec_N22 in A/B and RNBst_N22 in C/D titrated with dA(30). The panels on the left (A and C) are the raw data and represent the amount of power required to equilibrate temperature in the sample cell with that in the reference cell. The data points in the right panels (B and D) are the integrated power of the peaks in panels A and C, plotted as a function of the concentration of dA(30) in the sample cell.

power output to maintain a sample cell temperature equal to that of the reference cell. The dissociation constant defined for RNBec_N22 using ITC is 1.6µM, however, it also generates a standard deviation of 1.7µM (Figure 20A, B). Data obtained for RNBst_N22 revealed weaker binding, with a dissociation constant of 22.5µM with a standard deviation of 4.3µM (Figure 20C, D); this weaker affinity supports the qualitative data obtained from the RNase assays suggesting that RNBst_N22 is not as efficient as RNBec_N22 in degrading MS2 RNA. While these binding values are plausible, the magnitude of the error for RNBec_N22, is the same as the value obtained for the binding

constant, and means that this value is not as accurate a value as ITC can provide. Although the standard deviation for the dissociation constant of RNBst_N22 is smaller relative to the dissociation constant, in absolute terms, it is greater than that obtained from RNBec_N22. To maximize the power of ITC to generate accurate binding values, the standard deviation needs to be reduced. It is possible to increase the signal to noise ratio; however, the resources required to pursue this course of action limit this method's applicability.

3.4 Measurement of Binding by Electrophoretic Mobility Gel Shift Assay

A commonly used method for quantifying the binding of DNA/RNA to RNase II is monitoring a change in electrophoretic mobility of nucleic acid upon binding of substrate to RNase II. EMSA studies following binding of nucleic acids to RNase II typically use nucleic acids synthesized in the presence of [^{32}P]dUTP[αP], and the nucleic acid shift is visualized by autoradiography. One study in particular used SL9A, an 83nt synthetic, secondary structure containing RNA oligomer, and the naturally occurring *malE-malF* transcript (375nt), also containing secondary structure (Amblar et al., 2006). As this project was intended to avoid radioactivity, another sensitive method was needed in order to visualize a band shift. The band shift was followed by visualizing the protein shift using silver stain. After incubating 40μM RNBec_N22 with 400μM dA(30) for 10min in a 20μL sample volume, different volumes of the reaction sample were simultaneously analyzed using Native PAGE. In both the 2.5μL and 5μL loads, a faint band appears in the RNase II+dA(30) lane that has a lower mobility than the RNase II only lane (Figure 21). Although the new band indicates a binding event, there is not enough separation between the major and minor bands to accurately quantify densitometrically.

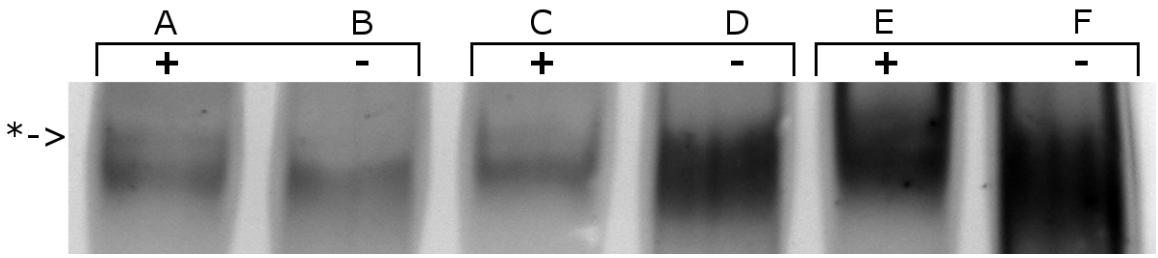
A
B
C
D
E
F
+
-
+
-
+
-
*->
Figure 21. Visualization of Binding by EMSA: Binding of RNase II to dA(30) oligomer visualized by electrophoretic mobility gel shift assay. All lanes are loaded with 40μM RNase II, with different amounts loaded. Lanes A and B have 100pmol RNase II, lanes C and D have 200pmol and lanes E and F have 400pmol. Plus and minus symbols indicate presence or absence of 400μM dA(30) ligand respectively. Asterisk at left of figure shows a shift in RNase II mobility.

3.5 Site-Directed Mutagenesis to Generate RNase II D209N Mutant

In a system where binding and catalysis are difficult to separate it is useful to have a catalytically inactive but otherwise unchanged mutant protein to remove the complication of catalytic steps from the measurement of binding events. In the case of RNase II, an inactive mutant has been reported, sequenced and purified (Amblar and Arraiano, 2005a, b), with the residue responsible for the loss of catalytic activity identified as 209. Residue 209 is an aspartate in wild-type RNase II and an asparagine in the catalytically inactive mutant. Despite the inability of the mutant – hereafter referred to as D209N – to degrade typical RNase II substrates, it retains the ability to bind these substrates with the same efficiency as wild-type RNase II. This mutant was generated to study the binding characteristics of RNase II.

Chapter 4: Discussion

4 Overview

The goal of this project is to improve the current model of RNase II structure and function. In particular, we aimed to use fluorescent methods to study the structural dynamics of RNase II as it degrades RNA in an effort to elucidate its processive catalytic function and mechanism. To this end, a series of RNase II C-terminal deletion mutants was generated and assayed for activity in order to establish a domain map. The information regarding the domain composition obtained from this approach would greatly facilitate the specific fluorescent labeling of sites in each domain in order to provide insight into the structural dynamics of RNase II using FRET.

The publication of three papers in rapid succession describing the domain composition and three dimensional structure of RNase II provided the opportunity to move directly into the development of a fluorescent system for studying structural dynamics. The paper by Amblar *et al* (2006) describes significant work with a C-terminal deletion mutant similar to RNBec_c60, and implicates the C-terminal S1 domain in RNA binding, while identifying a previously uncharacterized structural domain. The papers by Frazao *et al* (2006) and Zuo *et al.* (2006), describe the structure of RNase II at high resolution. These crystal structures show that the C-terminal deletion mutants generated here terminate at regions that are not inter-domain linkers, as predicted by the Scooby Domain server, but rather at various points within a complex multi-domain structure. The development of non-fluorescent assays was pursued concurrently in order to support and validate the results obtained using fluorescence.

4.1 C-Terminal Deletion Mutants

In order to generate a domain map of RNase II, a series of C-terminal deletion mutants was generated and assayed. The results of the activity assays were analyzed and the success of the prediction algorithm in selecting inter-domain regions was assessed. The publication of the X-ray crystallographic structure at the midpoint of the project allowed us to evaluate the initial set of C-terminal deletion mutants and carry on with the development of a FRET based system to study RNase II structural dynamics.

The C-terminal deletion mutants were generated by analyzing the output of the Scooby Domain inter-domain prediction server. The Scooby Domain successfully predicted the inter-domain region that was used when generating RNBec_c60. The design of this mutant was greatly facilitated by the presence of a structurally characterized domain that is homologous to the 60 C-terminal residues. Unlike RNBec_c60, the Scooby Domain server was not as successful at predicting inter-domain regions used when generating the larger C-terminal deletions. RNBec_c170 can fold and has been purified, in contrast, RNBec_c278 is only slightly soluble, and RNBec_c360 cannot be purified. According to the crystal structure, these mutants lack large sections of the RNB domain, likely contributing to their insolubility (see figure 8A-C).

The approach taken in designing these deletion mutants is reliable when considering that the majority of proteins have simple, contiguous domains. However, RNase II has complex domains and significant inter-domain interfaces. Due to these significant inter-domain interfaces, it is difficult to remove single, complete domains from these types of proteins.

In spite of the vast inter-domain interfaces, the crystal structure shows a domain composed of residues 418-472 and located within RNB domain. Zuo *et al.* – who published the crystal structure of RNase II one month after Frazao *et al.* (2006) – note that although this domain does not contain any of the conserved sequence motifs, it does form one wall of the catalytic pocket. It would be interesting to see if a deletion of this domain affects the exonucleolytic activity of RNase II. Additionally, Zuo *et al.* (2006) identify several positively charged residues (R535, R536, R539, R543) on the long α-helix that spans the distance between the RNB domain and the S1 domain that completes a basic ladder started by R500 and K501 of motif IV in the RNB domain. The effect of this helix on the processive mechanism of RNase II could be studied with RNBec_c170, the mutant in which this helix and motif IV (in which R500 and K501 are located) are absent, by another mutant that removes only the S1 domain and this helix, or by site-directed mutagenesis.

4.2 RNase Assays

In order to work towards generating a domain map of RNase II, the entire C-terminal S1 domain was targeted for deletion as described in the previous section. MS2 RNA hydrolysis by RNBec_c60 was analyzed using this RNase assay. The degradation of MS2 RNA by RNBec_c60 is significantly impaired compared to degradation by RNBec_N22. In order to degrade MS2 RNA to a similar extent as RNBec_N22, RNBec_c60 is required at a concentration ten times higher than RNBec_N22. Although there were no discrete degradation intermediates, the results of the RNase assay for RNBec_c60 show smearing directly beneath the main band that is not seen with the MS2 RNA degraded by either RNBec_N22 or RNBst_N22 (see figures 9A and 9B in results). This smearing is

likely caused by a decrease in the number of hydrolytic turnovers over which RNBec_c60 remains processive. Binding studies of a deletion mutant similar to RNBec_c60 shows that the binding of the deletion mutants is two to ten times weaker than the binding of the full-length RNase II (Amblar et al., 2006). Consequently, this impaired processivity is likely a result of a decrease in binding affinity.

The degradation of MS2 RNA by RNase II from two different organisms (*Salmonella typhimurium* – RNBst_N22; *Escherichia coli* – RNBec_N22) is largely similar; each enzyme processively degrades MS2 RNA molecules to completion at the same concentration over the same time. However, this RNase assay shows that RNBec_N22 converts full-length MS2 RNA to a species that is electrophoretically distinct from full-length MS2 RNA approximately two times faster than RNBst_N22. Over one hour, RNBec_N22 converts 75% of full-length MS2 RNA to a species electrophoretically distinct from full-length MS2 RNA compared to 40% converted by RNBst_N22. The source of this difference is unclear.

In addition to describing the qualitative properties of different RNase II proteins, a series of RNase assays using varying RNase II concentrations provide an association rate constant of $0.02 M^{-1} min^{-1}$ for the binding of MS2 RNA to RNase II. This is the first rate constant obtained for the association of RNase II to any nucleic acid to our knowledge; as a result it cannot be compared to any other values in the literature. Additionally, it provides an RNA turnover rate of approximately 6nt/s. The experimental design and assumption inherent in this calculation are likely to underestimate this turnover rate. Cannistraro and Kennell (1994) obtained a turnover rate of 70nt/s using polyadenylic acid, a synthetic homoribopolymer, as their substrate. Polyadenylic acid has no secondary

structure and is the preferred substrate of RNase II. Stretches of polyadenylate occur naturally in the cell, where they are synthesized at the 3' end of some mRNAs in a process which appears to play a role in gene regulation (Marujo et al., 2000). It is not presently clear whether polyadenylation increases or decreases gene expression as there have been conflicting reports that polyadenylation both destabilizes mRNA by targeting mRNA for degradation (Dreyfus and Regnier, 2002; Joanny et al., 2007), and stabilizes mRNA by RNase II-mediated removal of the 3' tail to which mRNA degradation machinery is proposed to bind (Marujo et al., 2000). Although polyadenylic acid is interesting when studying gene regulation, MS2 RNA, a physiological substrate and the target substrate in our RNase assay is interesting in that it more accurately represents the bulk RNA that RNase II would encounter *in vivo*. MS2 RNA does not have a 3' polyadenylate tail and has a relatively even distribution of the four ribonucleotides. The lack of a polyadenylate tail provides a sub-optimal binding target, while the distribution of the four ribonucleotides generates secondary structures through which RNase II must degrade. Each of these characteristics provides barriers to RNase II activity, leading to a lower RNA turnover rate than described by Cannistraro and Kennell (1999).

The rate of 6nt/s is nearly an order of magnitude lower than the rate at which mRNA is synthesized *in vivo*, which is 20-50nt/s (Voet and Voet, 2004). It is important that the rate of mRNA synthesis and exonucleolytic degradation closely balance each other, as a depletion of free nucleotides in the cell delays the production of gene products required by the cell at any given moment. This implies that the crude value obtained from our RNase assay is an underestimation while suggesting that the turnover rate of 70nt/s reported by Cannistraro and Kennell (1994) is an upper limit. Another enzyme that may

aid in balancing the synthesis and degradation of RNA in *E.coli* is Polynucleotide phosphorylase (PNPase), a phosphate dependant 3'-5' exoribonuclease. An additional factor in the slower RNA turnover rate measured here may have to do with the absence of an endoribonucleases in the system. It has been proposed that the endoribonuclease RNase E makes several cuts in an mRNA transcript during its degradation (Carpousis et al., 1999). It is to the 3' ends generated by this endonucleolytic cleavage that RNase II is proposed to bind and subsequently degrade (Carpousis et al., 1999)**.** Endoribonucleolytic cleavage of mRNA 5' to secondary structure elements would increase the RNA turnover rate by moving secondary structure to the 5' end of mRNA fragments, the point at which RNase II typically dissociates. The absence of an endoribonucleases likely slows the RNA turnover rate by forcing RNase II to degrade through secondary structure through which RNase II would not normally have to degrade.

Another factor leading to an underestimation of the RNA turnover rate compared to the previously published value is an assumption made in the analysis of the data. This assumption relates to the inability of this assay to observe dissociation. As a result, only binding events that result in degradation of MS2 RNA are measured. It is unlikely, however, that there is not dissociation in this system.

4.3 Binding Assays

4.3.1 Fluorescence Binding Assays

The development of a fluorescent binding assay was pursued by following the fluorescent emission of tryptophan, 5-IAF (thiol-specific label) and 2-AP (substrate) as well as by following the FRET between tryptophan and 5-IAF.

The binding assay following the tryptophan fluorescent upon addition of dA(30) to RNBec_N22 generates a dissociation constant of approximately 30μM. Subsequent experiments measuring the FRET between tryptophan and 5-IAF covalently linked to RNase II also generates a dissociation constant of around 30μM. A second look at the FRET results however, suggests that this value is an artifact.

Typically in FRET, there is an inverse correlation between the fluorescence of the donor and acceptor fluorophores; an increase in donor fluorescence accompanied by a decrease in acceptor fluorescence is characteristic of a decrease in FRET efficiency and is generally accepted to report an increase in distance between the fluorophores. Conversely, a decrease in donor fluorescence accompanied by an increase in acceptor fluorescence is characteristic of an increase in FRET efficiency, reporting a decrease in distance between the fluorophores. The FRET experiment conducted in this work reports neither of these events. Both the donor and acceptor fluorophores show a decrease in fluorescence upon addition of ligand to the system. In the FRET experiment conducted here the fluorescence of tryptophan is decreased by an alternative quenching event in the presence of dA(30).

Because the quenching appears as a function of increasing dA(30) concentration, the quenching must be related to the presence of dA(30). A search of the literature for adenylate-mediated quenching reveals that the quenching of tryptophan by adenine is a known phenomenon (Toulme et al., 1974). Titration of free L-tryptophan amino acids with dA(30) generates a dA(30) dependant change in tryptophan fluorescence nearly identical to that obtained by titrating dA(30) into RNase II. Therefore, the binding curves obtained in these experiments are due to the non-specific binding of dA(30) to RNase II,

which quenches tryptophan fluorescence, meaning that specific binding likely has a lower binding constant.

The results obtained from fluorescently labeling RNase II suggest that RNase II will not be susceptible to labeling with thiol-reactive fluorophores following the removal of a single cysteine residue (residue 603). A survey of the surface of RNase II suggests that there are four cysteines accessible to the solvent. When RNase II is shotgun labeled, the ratio of 5-IAF molecules to RNase II molecules is 0.6:1, suggesting that, on average, only one cysteine is accessible for covalent modification. Upon removal of this cysteine, other cysteines can be engineered into the RNase II sequence at discrete locations, allowing for fluorescent labeling and subsequent structural dynamic studies.

The use of 2-AP as a fluorophore was predicated on the properties of 2-AP in different conformational states. The substrate that was designed based on information from the crystal structure, containing a 2-AP base in the sixth residue from the 3' end, does not generate usable results. This outcome however, is not due to a conceptual flaw in the experimental setup, but rather indicates that optimization of this system is still required. There are still many positions within the RNA chain at which the 2-AP can be positioned. It is likely that the presence of 2-AP at one of these positions will generate usable results.

4.3.2 Isothermal Titration Calorimetry (ITC)

In order to complement the fluorescence binding studies, the binding of dA(30) to RNase II was also studied using ITC. This technique does not require a reporter group that may adversely affect enzyme activity and provides additional information regarding the thermodynamic properties associated with binding events.

RNase assays show that RNBec_N22 is able to convert full-length MS2 RNA to a species that is electrophoretically distinct from full-length MS2 RNA slightly faster than RNBst_N22. The ITC experiments show that the binding constant of RNBst_N22 (22.5μM) is approximately five times higher than that of RNBec_N22 (4.3μM), supporting the finding from the RNase assay. Although it is difficult to directly compare the results of ITC to the results of the RNase assay, the trend is the same.

Additionally, ITC experiments with RNBec_c60 show no binding at the same concentrations used with RNBec_N22 and RNBst_N22. This is also consistent with the results of the RNase assay, where RNBec_c60 is unable to degrade MS2 RNA at the same concentration that the full-length RNase II can. Again, this may be explained by two to tenfold drop in affinity between RNA and an RNase II mutant lacking its S1 domain (Amblar et al., 2006).

Although this technique will provide evidence to which the results from fluorescent binding studies can be compared, a full scale thermodynamic study of RNase II using ITC would be prohibitively expensive.

4.3.3 Electophoretic Mobility Gel Shift Assay (EMSA)

The results of the EMSA studies provide additional support that there is binding at the concentrations used. Despite its extensive use in the literature, EMSA is not a true equilibrium technique, and is not ideal for the quantitative analysis of binding. Rather it is useful for obtaining an estimate of the range of concentrations in which binding occurs. This is not a true equilibrium technique because electrophoresis separates the complex from unbound RNase II and RNA. The shift of the system away from equilibrium

presents the opportunity for complex dissociation, therefore underestimating the binding constant.

4.4 Future Directions

Following the goal of this project, work will be continued to develop a system to measure the structural dynamics of RNase II using fluorescence. By utilizing a combination of intramolecular and intermolecular FRET dye pairs, it will be possible to describe binding, hydrolysis and translocation at a molecular level. The knowledge garnered from the publication of the high resolution structure of RNase II provides a valuable starting point in designing proteins that can be labeling at positions for the study of a variety of RNase II properties.

4.4.1 Binding Assay

The development of a fluorescent binding assay can continue by utilizing currently available materials. At present, RNase II labeled with 5-IAF and dA(30) labeled with 2-AP are available. FRET between these dyes would provide a low background binding assay, and would be the next system to test, however, time constraints prevented a study of this system.

As is the case in the spectral overlap between tryptophan and 5-IAF, the spectral overlap between 2-AP and 5-IAF is not optimal (Figure 22). However, the results from the FRET experiments suggest that there may be sufficient energy transferred to measure through acceptor fluorescence. In this experiment, the dA(30)-2-AP can be excited, and only when it is bound to RNBec_N22*5IAF, will it transfer energy, resulting in RNBec_N22*5IAF fluorescence. As the transfer of energy will only happen when the ligand is bound to RNase II, fluorescein emission will be a more sensitive reporter of

binding events. Additionally, the issue of background fluorescence will not complicate the data, as the measurement of the light emitted at the emission maxima of 5-IAF will not detect the fluorescence of the increasing concentrations of 2-AP. As is the case with tryptophan and 5-IAF, the overlap integral between 2-AP and 5-IAF is not optimal, however it does provide a potential method for detecting the binding of nucleic acid to protein by only providing a change in signal when the two fluorophores come into close proximity to one another (under 100Å).

5-IAF bound to RNase II is not sensitive to the addition of dA(30), and the overlap integral with tryptophan required for FRET is very small. An alternative dye that is more frequently used in FRET studies in conjunction with tryptophan is 5-((((2-iodoacetyl)amino)ethyl)amino)naphthalene-1-sulfonic acid (IAEDANS). IAEDANS has an absorbance maximum of 356nm, which provides a larger overlap integral when paired with tryptophan. However, it has already been shown that tryptophan fluorescence is quenched by dA(30). Rather than using the compromised tryptophan fluorescence, an alternative donor fluorophore may be used. As dA(30)-2-AP

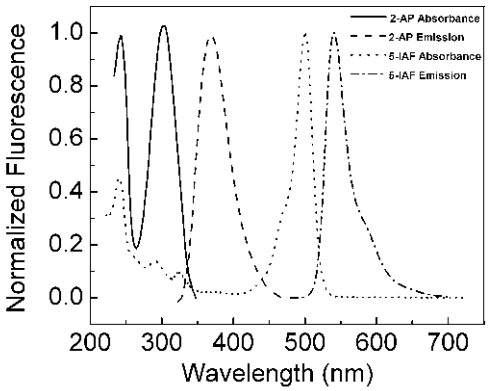

Figure 22. Spectra of 2-AP and 5-IAP: Spectral overlap between 2-aminopurine and 5-iodoacetamidofluorescein

is already available, it would be a suitable choice as a donor fluorophore. In addition, this type of system will provide the benefit of visualizing acceptor fluorescence only in cases where the donor fluorophore is within molecular proximity of the acceptor, which in this case is a binding event.

Another alternative binding assay is to analyze data obtained in quenching experiments with modified Stern-Volmer plots (Lakowicz, 1999). These plots measure the fractional accessibility of fluorophores in solution, and if the concentrations are known, can be extended to determine the number of fluorophores that are unquenched. A series of experiments at increasing dA(30)-2-AP concentrations, measuring the effects of a quenching agent on the fluorescence of dA(30)-2-AP in the presence of RNase II and its mutants, can potentially describe the quantity of dA(30)-2-AP bound to RNase II, and may provide sufficient data to describe the binding affinity for each of these variants

The binding may be observed using a property of fluorescence that is distinct from its intensity. This property, fluorescence anisotropy is a measure of how fast a molecule tumbles in solution. This value is obtained by measuring the polarization of emitted light from a fluorophore that has been excited by polarized light. The fluorescence anisotropy of dA(30)-2-AP could be measured before and after binding to RNase II. A binding event between the relatively small dA(30)-2-AP and the larger RNase II would decrease the freedom dA(30)-2-AP has to tumble, significantly increasing the anisotropy of the fluorophore.

Once an appropriate fluorescent binding assay has been developed, the project can move forward to study the structural dynamics of RNase II.

4.4.2 Kinetics

Following the development of a fluorescence based binding assay and subsequent confirmation with non-fluorescent methods, the next goal in this project would be to characterize the kinetics of binding, such as association and dissociation rate constants. The kinetics of association and dissociation to a variety of substrates, ranging from polyadenylate, the preferred substrate of RNase II, to precursor tRNAs and rRNAs will provide insight into the *in vivo* function of RNase II. Specifically, these values may help in elucidating the role of RNase II in processing and degradative RNA hydrolysis. Association and dissociation events can be followed by utilizing the fluorescent system previously developed for the binding studies in a stopped-flow apparatus.

In addition, the project will move towards the study of RNA degradation, and the mechanisms associated with degradation, by RNase II. The literature presents little data regarding the rates at which RNase II hydrolyzes RNA. There is even less data regarding the rates of binding, translocation and dissociation between RNase II and physiological substrates. RNase II has been shown to remove nucleotides from an RNA chain at a rate of 70nt/s (Cannistraro and Kennell, 1994). Another study suggests that the binding, translocation and dissociation events add up to a time of 1.46s (Coburn and Mackie, 1996b). The fluorescent system will allow us to assess the contribution of binding, translocation and dissociation to the 1.46s value.

Next to binding, the kinetics of RNA hydrolysis will be the simplest mechanism to visualize. 2-AP promises to be a very powerful probe in visualizing RNA hydrolysis. 2-AP is reported to be 100 times more fluorescent as a part of a ribonucleoside monophosphate than when it is a member of an RNA chain (Ward et al., 1969). 2-AP can

be incorporated into different positions in RNA, and the time required for an increase in fluorescent signal could be quantified.

RNase II can bind, but not degrade ssDNA (Gorelic and Apirion, 1971; Singer and Tolbert, 1965; Spahr, 1964). This property of RNase II makes the study of translocation possible. By incorporating ssDNA into a chimeric polynucleotide consisting of ribonucleotides at the 3' end, the processive hydrolysis can be arrested, allowing for a study of translocation once the kinetics of hydrolysis have been defined. In addition to the kinetics of binding, hydrolysis, and translocation, the dynamic movements of RNase II associated with each of these steps can be studied, and will be the subject of long-term studies.

4.4.3 Outstanding Long-Term Questions

The binding and kinetics studies suggested in the previous two sections will eventually address some of the large scale questions regarding the structure and function of RNase II. Some of these unanswered questions lingering in the literature include the mechanism whereby RNA is translocated into the catalytic pocket and the interactions between RNA and RNase II at the anchor region during RNA hydrolysis.

The number of domains in RNase II allows for a number of mutants to be generated in which the relative movement of two domains can be studied through FRET. For example, it has been proposed that a catalytic region and an anchor region move relative to one another (Cannistraro and Kennell, 1999) during RNA hydrolysis. The crystal structure shows two regions of contact with RNA. By specifically labeling domains within RNase II, these proposed intramolecular movements can be characterized. Not only can the movement of the catalytic region relative to the anchor region be compared, the

movement between the domains composing the anchor region can be studied. This will allow us to determine if the domains in the anchor region move together in a concerted mechanism, or separately in a sequential mechanism to advance RNA into the catalytic pocket.

In these types of studies, it is unlikely that RNase II's intrinsic tryptophans will be appropriate as a partner in a FRET dye pair due to the relatively high number of tryptophans (nine) in RNase II. The movement of some tryptophans towards the acceptor dye and some away from the acceptor dye will greatly complicate the signal interpretation. Instead, the introduction of a pair of cysteines into RNase II following the removal of C603 will allow RNase II to be labeled with a common FRET pair such as Cy3/Cy5, simplifying the interpretation of FRET signals. This type of system is ideal in studying the translocation of RNA into the RNase II active site. Additionally, this will help to uncover which of two types of interactions proposed by Cannistraro and Kennell (1999) are occurring at the anchor region of RNase II during hydrolysis. The first interaction is a sliding movement, where, as nucleotides are removed from the 3' end of the RNA chain, the RNA chain slides through the anchor region. The alternative proposal suggests that the RNA remains bound to the anchor region of RNase II while nucleotides are being removed from the 3' end. During these progressive removals, the RNA not bound between the catalytic region and anchor region stretch until they reach a critical point, where they briefly lose contact with the anchor region and re-associate 5' to its original binding position.

In addition to the intramolecular questions posed above, translocation can be studied using intermolecular interactions. There are reports that RNase II has vital contacts with

RNA at a site that is 17-27 nucleotides from the 3' end (Cannistraro and Kennell, 1999). However, the crystal structure of an inactive RNase II shows a 13 nucleotide RNA oligomer bound to RNase II (Frazao et al., 2006). The presence of 13 nucleotides was not by design; the RNA fortuitously co-purified with the inactive RNase II mutant. If, as suggested by Cannistraro and Kennell, there are important contacts 17-27 nucleotides from the 3' end of the RNA, why are they not present in the structure? This question can be addressed by incorporating 2-AP a fluorescent adenine analogue into an RNA oligomer. By placing the 2-AP dye at a point greater than 27 nucleotides from the 3' end, and an appropriate acceptor dye on the anchor region, the proximity of these dyes can be monitored through FRET efficiency.

4.5 Conclusion

In this work, we have used an RNase assay with a previously unstudied substrate to generate information about RNase II, an orthologue of RNase II and a deletion mutant of RNase II. In addition, we have completed work towards developing a fluorescently based binding assay to be used in future studies of structural dynamics.

The RNase assay generated an association rate constant of $0.02M^{-1}min^{-1}$, which is the first association rate constant to be generated for RNase II. In addition, the RNase assay has shown that RNBec_N22 degrades MS2 RNA faster than RNBst_N22, which is likely a result of a lower binding affinity, as shown by ITC studies. Furthermore, we have shown that RNBec_c60, while active, has a greatly reduced binding affinity, which aggress with the previously published information that the removal of the C-terminal domain reduces the affinity of RNase II to RNA two to tenfold (Amblar et al., 2006).

We have made progress towards developing a fluorescence based binding assay for use in future structural dynamic studies. We have attempted to use intrinsic protein fluorescence, shotgun labeled protein fluorescence, and substrate fluorescence to observe binding between RNase II and an RNA analogue. Although none of these alone was able to generate a reliable binding curve, it appears that a fluorescent binding assay is imminent.

The structural dynamics studies will also benefit from information gathered from the shotgun labeling of RNase II. The results from shotgun labeling RNase II suggest that on average, only one cysteine is labeled. An examination of the solvent accessible surface of RNase II suggests that this residue is C603. With this information, we know that we only need to remove a single cysteine residue (out of seven total) before we are able to engineer cysteines into specific locations on RNase II for use in structural dynamic studies.

The work described here, along with the X-ray crystal structures of RNase II has allowed us to take a significant step towards studying the structural dynamics of RNase II.

Sources Cited

Abramoff, M.D., Magelhaes, P.J., and Ram, S.J. (2004). Image Processing with ImageJ. Biophotonics International *11*, 36-42.

Amblar, M., and Arraiano, C.M. (2005a). (Corrigendum) A single mutation in *Escherichia coli* Ribonuclease II inactivates the enzyme without affecting RNA binding. (vol 272, pg 363, 2005). FEBS Journal *272*, 2345.

Amblar, M., and Arraiano, C.M. (2005b). A single mutation in *Escherichia coli* Ribonuclease II inactivates the enzyme without affecting RNA binding. FEBS Journal *272*, 363-374.

Amblar, M., Barbas, A., Fialho, A.M., and Arraiano, C.M. (2006). Characterization of the functional domains of *Escherichia coli* RNase II. Journal of Molecular Biology *360*, 921-933.

Apirion, D. (1978). Isolation, Genetic Mapping and Some Characterization of a Mutation in *Escherichia coli* That Affects the Processing of Ribonucleic Acid. Genetics, 659-671.

Barbas, A., Matos, R.G., Amblar, M., Lopez-Vinas, E., Gomez-Puertas, P., and Arraiano, C.M. (2008). New Insights into the Mechanism of RNA Degradation by Ribonuclease II: Identification of the Residue Responsible for Setting the RNase II End-Product. The Journal of Biological Chemistry.

Bouvet, P., and Belasco, J.G. (1992). Control of RNase E-mediated RNA degradation by 5[prime]-terminal base pairing in *E. coli*. Nature *360*, 488-491.

Bradford, M.M. (1976). A rapid and sensitive method for the quantitation of microgram quantities of protein utilizing the principle of protein-dye binding. Analytical Biochemistry *72*, 248-254.

Brodsky, L.I., Ivanov, V.V., Kalaidzidis, Y.L., Leontovich, A.M., Nikolaev, V.K., Feranchuk, S.I., and Drachev, V.A. (1995). GeneBee-NET: Internet-based server for analyzing biopolymers structure. Biochemistry *60*, 923-928.

Brodsky, L.I., Vasiliev, A.V., Kalaidzidis, Y.L., Osipov, Y.S., Tatuzov, R.L., and Feranchuk, S.I. (1992). GeneBee: the program package for biopolymer structure analysis. Dimacs *8*, 127-139.

Cannistraro, V.J., and Kennell, D. (1994). The Processive Reaction-Mechanism of Ribonuclease-II. Journal of Molecular Biology *243*, 930-943.

Cannistraro, V.J., and Kennell, D. (1999). The reaction mechanism of Ribonuclease II and its interaction with nucleic acid secondary structures. Biochimica Et Biophysica Acta-Protein Structure and Molecular Enzymology *1433*, 170-187.

Carpousis, A.J., Vanzo, N.F., and Raynal, L.C. (1999). mRNA degradation: a tale of poly(A) and multiprotein machines. Trends in Genetics *15*, 24-28.

Chaney, S.G., and Boyer, P.D. (1972). Incorporation of water oxygens into intracellular nucleotides and RNA : II. Predominantly hydrolytic RNA turnover in *Escherichia coli*. Journal of Molecular Biology *64*, 581-561.

Cheng, Z.-F., Zuo, Y., Li, Z., Rudd, K.E., and Deutscher, M.P. (1998). The *vacB* Gene Required for Virulence in *Shigella flexneri* and *Escherichia coli* Encodes the Exoribonuclease RNase R. The Journal of Biological Chemistry *273*, 14077-14080.

Cheng, Z.F., and Deutscher, M.P. (2002). Purification and characterization of the *Escherichia coli* exoribonuclease RNase R - Comparison with RNase II. Journal of Biological Chemistry *277*, 21624-21629.

Coburn, G.A., and Mackie, G.A. (1996a). Differential sensitivities of portions of the mRNA for ribosomal protein S20 to 3'-exonucleases dependent on oligoadenylation and RNA secondary structure. Journal of Biological Chemistry *271*, 15776-15781.

Coburn, G.A., and Mackie, G.A. (1996b). Overexpression, purification, and properties of *Escherichia coli* Ribonuclease II. Journal of Biological Chemistry *271*, 1048-1053.

Cudny, H., and Deutscher, M.P. (1980). Apparent involvement of Ribonuclease D in the 3' processing of transfer-RNA precursors. Proceedings of the National Academy of Sciences of the United States of America-Biological Sciences *77*, 837-841.

Deutscher, M.P., Marshall, G.T., and Cudny, H. (1988). RNase PH: An *Escherichia coli* phosphate dependant nuclease distinct from polynucleotide phosphorylase. Proceedings of the National Academy of Sciences of the United States of America *85*, 4710-4714.

Deutscher, M.P., and Reuven, N.B. (1991). Enzymatic basis for hydrolytic versus phosphorolytic messenger-RNA degradation in *Escherichia coli* and *Bacillus subtilis.* Proceedings of the National Academy of Sciences of the United States of America *88*, 3277-3280.

Donovan, W.P., and Kushner, S.R. (1986). Polynucleotide Phosphorylase and ribonuclease II are required for cell viability and mRNA turnover in *Escherichia coli* K-12. Proceedings of the National Academy of Sciences of the United States of America *83*, 120-124.

Dreyfus, M., and Regnier, P. (2002). The Poly(A) Tail of mRNAs: Bodyguard in Eukaryotes, Scavenger in Bacteria. Cell *111*, 611-613.

Dunn, J.J., and Studier, F.W. (1973). T7 Early RNAs and *Escherichia coli* Ribosomal RNAs are Cut from Large Precursor RNAs *In Vivo* by Ribonuclease III. Proceedings of the National Academy of Sciences of the United States of America *70*, 3296-3300.

Dziembowski, A., Lorentzen, E., Conti, E., and Seraphin, B. (2007). A single subunit, Dis3, is essentially responsible for yeast exosome core activity. Nature Structural and Molecular Biology *14*, 15-22.

Erova, T.E., Kosykh, V.G., Fadl, A.A., Sha, J., Horneman, A.J., and Chopra, A.K. (2008). Cold Shock Exoribonuclease R (VacB) Is Involved in *Aeromonas hydrophila* Pathogenesis. Journal of Bacteriology *190*, 3467-3474.

Evguenieva-Hackenberg, E., Walter, P., Hochleitner, E., Lottspeich, F., and Klug, G. (2003). An exosome-like complex in *Sulfolobus solfataricus*. EMBO Reports *4*, 889-893.

Fersht, A. (1999). Structure and Mechanism in Protein Science: A Guide to Enzyme Catalysis and Protein Folding (New York: W. H. Freeman and Company), 631.

Fiers, W., Contreras, R., Duerinck, F., Haegeman, G., Iserentant, D., Merregaert, J., Min Jou, W., Molemans, F., Raeymaekers, A., Van den Berghe, A., *et al.* (1976). Complete nucleotide sequence of bacteriophage MS2 RNA: primary and secondary structure of the replicase gene. Nature *260*, 500-507.

Frazao, C., McVey, C.E., Amblar, M., Barbas, A., Vonrhein, C., Arraiano, C.M., and Carrondo, M.A. (2006). Unravelling the dynamics of RNA degradation by ribonuclease II and its RNA-bound complex. Nature *443*, 110-114.

Gasteiger, E., Hoogland, C., Gattiker, A., Duvand, S., Wilkins, M.R., Appel, R.D., and Bairoch, A. (2005). Protein Identification and Analysis Tools on the ExPASy Server. In The Proteomics Protocols Handbook, J.M. Walker, ed. (Totowa: Humana Press), 571-607.

George, R.A., Lin, K., and Heringa, J. (2005). Scooby-domain: prediction of globular domains in protein sequence. Nucleic Acids Research *33*, 160-163.

Goodrich, J.A., and Kugel, J.F. (2007). Binding and Kinetics for Molecular Biologists (Cold Spring Harbor: Cold Spring Harbor Laboratory Press), 182.

Gorelic, L., and Apirion, D. (1971). Inhibition of RNase II by DNA. Biochemical and Biophysical Research Communications *44*, 1184-1191.

Gupta, R.S., Kasai, T., and Schlessinger, D. (1977). Purification and Some Novel Properties of *Escherichia coli* RNase II. Journal of Biological Chemistry *252*, 8945-8949.

Joanny, G., Le Derout, J., Brechemier-Baey, D., Labas, V., Vinh, J., Regnier, P., and Hajnsdorf, E. (2007). Polyadenylation of a functional mRNA controls gene expression in *Escherichia coli*. Nucleic Acids Research *35*, 2494-2502.

Kapakos, J.G., and Steinberg, M. (1982). Fluorescent labeling of (Na+ & K+)-ATPase by 5-iodoacetamidofluorescein. Biochimica et Biophysica Acta (BBA) - Biomembranes *693*, 493-496.

Kaplan, R., and Apirion, D. (1974). Involvement of Ribonuclease-I, Ribonuclease-II, and Polynucleotide Phosphorylase in Degradation of Stable Ribonucleic-Acid During Carbon Starvation in *Escherichia coli*. Journal of Biological Chemistry *249*, 149-151.

Kelly, K.O., and Deutscher, M.P. (1992a). Characterization of RNase PH. The Journal of Biological Chemistry *267*, 17153-17158.

Kelly, K.O., and Deutscher, M.P. (1992b). The presence of only one of 5 exoribonucleases is sufficient to support the growth of *Escherichia coli.* Journal of Bacteriology *174*, 6682-6684.

Kelly, K.O., Reuven, N.B., Li, Z., and Deutscher, M.P. (1992). RNase PH is Essential for tRNA Processing and Viability in RNase-Deficient *Escherichia coli* Cells. The Journal of Biological Chemistry *267*, 16015-16018.

Kennell, D. (2002). Processing Endoribonucleases and mRNA Degradation in Bacteria. Journal of Bacteriology *184*, 4645-4657.

Kivity-Vogel, T., and Elson, D. (1968). A correlation between Ribonuclease II and the *in vivo* inactivation of messenger RNA in *E.coli*. Biochemical and Biophysical Research Communications *33*, 412-417.

Koonin, E.V., Wolf, Y.I., and Aravind, L. (2001). Prediction of the Archaeal Exosome and Its Connections with the Proteasome and the Translation and Transcription Machineries by a Comparative-Genomic Approach. Genome Reseach *11*, 240-252.

Kushner, S.R. (2002). mRNA Decay in *Escherichia coli* Comes of Age. Journal of Bacteriology *184*, 4658-4665.

Kuwano, M., Ono, M., Endo, H., Hori, K., Nakamura, K., Hirota, Y., and Ohnishi, Y. (1977). Gene affecting longevity of messenger RNA: a mutant of *Escherichia coli* with altered mRNA stability. Molecular & General Genetics *154*, 279-285.

Laemmli, U.K. (1970). Cleavage of Structural Proteins during the Assembly of the Head of Bacteriophage T4. Nature *277*, 680-685.

Lakowicz, J.R. (1999). Principles of fluorescence spectroscopy, 2nd edn (New York: Springer Science+Business Media), 698.

Layne, E. (1957). Spectrophotometric and Turbidimetric Methods for Measuring Proteins. Methods in Enzymology *3*, 477-455.

Li, Z.W., and Deutscher, M.P. (1995). The transfer-RNA processing enzyme RNase T is essential for maturation of 5S RNA. Proceedings of the National Academy of Sciences of the United States of America *92*, 6883-6886.

Li, Z.W., Pandit, S., and Deutscher, M.P. (1999). Maturation of 23S ribosomal RNA requires the exoribonuclease RNase T. RNA-A Publication of the RNA Society *5*, 139-146.

Liu, Q., Greimann, J.C., and Lima, C.D. (2006). Reconstitution, Activities, and Structure of the Eukaryotic RNA Exosome. Cell *127*, 1223-1237.

Lorentzen, E., Basquin, J., Tomecki, R., Dziembowski, A., and Conti, E. (2008). Structure of the Active Subunit of the Yeast Exosome Core, Rrp44: Diverse Modes of Substrate Recruitment in the RNase II Nuclease Family. Molecular Cell *29*, 717-728.

Lorentzen, E., and Conti, E. (2005). Structural Basis of 3' End RNA Recognition and Exoribonucleolytic Cleavage by and Exosome RNase PH Core. Molecular Cell *20*, 473-481.

Lorentzen, E., Dziembowski, A., Lindner, D., Seraphin, B., and Conti, E. (2007). RNA channelling by the archaeal exosome. EMBO Reports *8*, 470-476.

Lorentzen, E., Walter, P., Fribourg, S., Evguenieva-Hackenberg, E., Klug, G., and Conti, E. (2005). The archaeal exosome core is a hexameric ring structure with three catalytic subunits. Nature Structural and Molecular Biology *12*, 575-581.

Malta, E., Moolenaar, G.F., and Goosen, N. (2006). Base Flipping in Nucleotide Excision Repair. Journal of Biological Chemistry *281*, 2184-2194.

Marujo, P.E., Hajnsdorf, E., Le Derout, J., Andrade, R., Arraiano, C.M., and Regnier, P. (2000). RNase II removes the oligo(A) tails that destabilize the rpsO mRNA of *Escherichia coli*. RNA-A Publication of the RNA Society *6*, 1185-1193.

Mian, I.S. (1997). Comparative sequence analysis of Ribonucleases HII, III, II PH and D. Nucleic Acids Research *25*, 3187-3195.

Mitchell, P., Petfalski, E., Shevchenko, A., Mann, M., and Tollervey, D. (1997). The Exosome: A Conserved Eukaryotic RNA Processing Complex Containing Multiple 3'-5' Exoribonucleases. Cell *91*, 457-466.

Mohanty, B.K., and Kushner, S.R. (2000). Polynucleotide phosphorylase, RNase II and RNase E play different roles in the in vivo modulation of polyadenylation in *Escherichia coli*. Molecular Microbiology *36*, 982-994.

Mohanty, B.K., and Kushner, S.R. (2003). Genomic analysis in *Escherichia coli* demonstrates differential roles for polynucleotide phosphorylase and RNase II in mRNA abundance and decay. Molecular Microbiology *50*, 645-658.

Navarro, M.V.A.S., Oliveira, C.C., Zanchin, N.I.T., and Guimaraes, B.G. (2008). Insights into the Mechanism of Progressive RNA Degradation by the Archaeal Exosome. The Journal of Biological Chemistry *283*, 14120-14131.

Nossal, N.G., and Singer, M.F. (1968). Processive Degradation of Individual Polyribonucleotide Chains I. *Escherichia Coli* Ribonuclease 2. Journal of Biological Chemistry *243*, 913-922.

Ono, M., and Kuwano, M. (1979). A conditional lethal mutation in an *Escherichia coli* strain with a longer chemical lifetime of messenger RNA. Journal of Molecular Biology *129*, 343-357.

Pang, C.N., Lin, K., Wouters, M.A., Heringa, J., and George, R.A. (2008). Identifying foldable regions in protein sequence from the hydrophobic signal. Nucleic Acids Research *36*, 578-588.

Reuven, N.B., and Deutscher, M.P. (1993). Multiple Exoribonucleases required for the 3'-processing of *Escherichia coli* tRNA precursors *in vivo*. The FASEB Journal *7*, 143-148.

Singer, M.F., and Tolbert, G. (1964). Specificity of Potassium-Activated Phosphodiesterase of *Escherichia coli*. Science *145*, 593-595.

Singer, M.F., and Tolbert, G. (1965). Purification and Properties of a Potassium-Activated Phosphodiesterase (RNAase 2) from *Escherichia coli*. Biochemistry *4*, 1319-1330.

Spahr, P.F. (1964). Purification and Properties of Ribonuclease 2 from *Escherichia coli*. Journal of Biological Chemistry *239*, 3716-3726.

Spahr, P.F., and Schlessinger, D. (1963). Breakdown of Messenger Ribonucleic Acid by a Potassium-Activated Phosphodiesterase from *Escherichia coli*. Journal of Biological Chemistry *238*, 2251-2253.

Spickler, C., and Mackie, G.A. (2000). Action of RNase II and polynucleotide phosphorylase against RNAs containing stem-loops of defined structure. Journal of Bacteriology *182*, 2422-2427.

Stoschek, C.M. (1990). Quantitation of Protein. Methods in Enzymology *182*, 50-69.

Tobe, T., Sasakawa, C., Okada, N., Honma, Y., and Yoshikawa, M. (1992). *vacB*, a Novel Chromosomal Gene Required for Expression of Virulence Genes on the Large Plasmid of *Shigella flexneri*. Journal of Bacteriology *174*, 6359-6367.

Toulme, J.-J., Charlier, M., and Helene, C. (1974). Specific Recognition of Single-Stranded Regions in Ultraviolet-Irradiated and Heat-Denatured DNA by Tryptophan-Containing Peptides. Proceedings of the National Academy of Sciences of the United States of America *71*, 3185-3188.

Vanzo, N.F., Li, Y.S., Py, B., Blum, E., Higgins, C.F., Raynal, L.C., Krisch, H.M., and Carpousis, A.J. (1998). Ribonuclease E organizes the protein interactions in the *Escherichia coli* RNA degradosome. Genes and Development *12*, 2770-2781.

Voet, D., and Voet, J.G. (2004). Biochemistry. (John G. Wiley and Sons), 1228.

Wang, H.-W., Wang, J., Ding, F., Callahan, K., Bratkowski, M.A., Butler, J.S., Nogales, E., and Ke, A. (2007). Architecture of the yeast Rrp44-exosome complex suggests routes of RNA recruitment for 3' end processing. Proceedings of the National Academy of Sciences of the United States of America *104*, 16844-16849.

Ward, D.C., Reich, E., and Stryer, L. (1969). Fluorescence studies of nucleotides and polynucleotides I. Formycin, 2-aminopurine riboside, 2,6-diaminopurine riboside, and their derivatives. Journal of Biological Chemistry *244*, 1228-1237.

Weaver, R.F. (2002). Molecular Biology, 2nd edn (New York
McGraw Hill).

Young, R.A., and Steitz, J.A. (1978). Complementary sequences 1700 nucleotides apart form a ribonuclease III cleavage site in *Escherichia coli* ribosomal precursor RNA. Proceedings of the National Academy of Sciences of the United States of America *75*, 3593-3597.

Zhang, J., and Deutscher, M.P. (1988). Transfer-RNA is a substrate for RNase D *in vivo*.. Journal of Biological Chemistry *263*, 17909-17912.

Zhou, Z., and Deutscher, M.P. (1997). An Essential Function for the Phosphate-Dependant Exoribonuclease RNase PH and Polynucleotide Phosphorylase. Journal of Bacteriology *179*, 4391-4395.

Zukin, R.S., Hartig, P.R., and Koshland Jr., D.E. (1977). Use of a distant reporter group as evidence for a conformational change in a sensory receptor. Proceedings of the National Academy of Sciences of the United States of America *74*, 1932-1936.

Zuo, Y.H., Vincent, H.A., Zhang, J.W., Wang, Y., Deutscher, M.P., and Malhotra, A. (2006). Structural basis for processivity and single-strand specificity of RNase II. Molecular Cell *24*, 149-156.

Appendix A – Equations

Curve-fitting of Association Rate Data – Used in Section 3.1.2

$$y = A\cdot(1-\exp(-B\cdot x))+C$$

Where: y is the fraction of substrate remaining
x is time
A is the amount of substrate at time = 0
B is the apparent rate constant
C is the amount of substrate at time = ∞

Curve-fitting of Binding Curves – Used in Sections 3.2.1, 3.2.3, 3.2.4, 3.3

$$y = (A+(B\cdot x))/(C+x)$$

Where: y is the signal generated (fluorescence or power)
x is the substrate concentration
A is the fluorescence (or power) when substrate concentration = 0
B is the fluorescence (or power) when substrate concentration = ∞
C is the binding constant

Quantum Yield – Referenced in Section 3.2

$$Q = \Gamma/(\Gamma+k_{nr})$$

Where: Q is the quantum yield
Γ is the emissive rate of the fluorophore
k_{nr} is the rate of nonradiative decay

FRET Efficiency – Referenced in Section 3.2.3

$$E = 1/(1+(r^6/R_o^6))$$

Where: E is the FRET efficiency
r is the distance separating the fluorophores
R_o is the Förster distance

Förster Distance (R_o) – Referenced in Section 3.2.3

$$R_o = (9000 \cdot (\ln 10) \cdot \kappa^2 \cdot Q_d \cdot J)/(128 \cdot \pi^5 \cdot n^4 \cdot N_{av})$$

Where: κ^2 is the orientation factor of the fluorophores (set at 2/3 in FRET)
Q_d is the quantum yield of the donor fluorophore
J is the overlap integral
N_{av} is Avogadro's number
n is the refractive index of the medium.